KTH Computer Science
and Communication

Adaptive Algorithms and High Order Stabilization for Finite Element Computation of Turbulent Compressible Flow

MURTAZO NAZAROV

Doctoral Thesis
Stockholm, Sweden 2011

TRITA-CSC-A 2011:13
ISSN-1653-5723
ISRN-KTH/CSC/A–11/13-SE
ISBN 978-91-7501-053-3

KTH, CSC
SE-100 44 Stockholm
SWEDEN

Akademisk avhandling som med tillstånd av Kungl Tekniska högskolan framlägges till offentlig granskning för avläggande av teknologie doctorexamen Torsdagen den 1 Sep 2011 klockan 10.00 i sal F3, Lindstedtsvägen 26 Entreplan, Kungliga Tekniska högskolan, Stockholm.

Tryck: E-print, www.eprint.se

To my father Zoidjon and
my mother Muhabbat

Abstract

This work develops finite element methods with high order stabilization, and robust and efficient adaptive algorithms for Large Eddy Simulation of turbulent compressible flows.

The equations are approximated by continuous piecewise linear functions in space, and the time discretization is done in implicit/explicit fashion: the second order Crank-Nicholson method and third/fourth order explicit Runge-Kutta methods. The full residual of the system and the entropy residual, are used in the construction of the stabilization terms. These methods are consistent for the exact solution, conserves all the quantities, such as mass, momentum and energy, is accurate and very simple to implement. We prove convergence of the method for scalar conservation laws in the case of an implicit scheme. The convergence analysis is based on showing that the approximation is uniformly bounded, weakly consistent with all entropy inequalities, and strongly consistent with the initial data. The convergence of the explicit schemes is tested in numerical examples in 1D, 2D and 3D.

To resolve the small scales of the flow, such as turbulence fluctuations, shocks, discontinuities and acoustic waves, the simulation needs very fine meshes. In this thesis, a robust adjoint based adaptive algorithm is developed for the time-dependent compressible Euler/Navier-Stokes equations. The adaptation is driven by the minimization of the error in quantities of interest such as stresses, drag and lift forces, or the mean value of some quantity.

The implementation and analysis are validated in computational tests, both with respect to the stabilization and the duality based adaptation.

Preface

This thesis consists of an introduction and six papers. The overview of the papers is given in the introduction. The papers are included in the second part of the thesis.

Paper I.

Jean-Luc Guermond, Murtazo Nazarov and Bojan Popov. Implementation of the entropy viscosity method. *Technical report, kth-ctl-4015,* 2011.

The author of this thesis contributed with the ideas and writing of the manuscript, and performed the numerical implementation of the compressible Euler computations.

Paper II.

Murtazo Nazarov. Convergence of a residual based artificial viscosity finite element method. *Technical report, kth-ctl-4016,* 2011.

The author of the thesis came up to the ideas, performed the proofs and the numerical implementations.

Paper III.

Murtazo Nazarov and Johan Hoffman. An adaptive finite element method for inviscid compressible flow. *International Journal for Numerical Methods in Fluids* 2010; **64**(10-12):1102–1128.

The author of this thesis contributed to the ideas, wrote the manuscript and performed the implementations. The author presented a part of this work

at the FEF '09 conference, Tokyo, Japan, and at the Finite Element Rodeo'10, Dallas, USA.

Paper IV.

Murtazo Nazarov, Jean-Luc Guermond and Bojan Popov. A posteriori error estimation for the compressible Euler equations using entropy viscosity. *Technical report, kth-ctl-4017,* 2011.

The author of the thesis contributed to the ideas and he carried out the theoretical developments, performed the numerical implementations and wrote the manuscript. The author presented a part of this work at the FEF '11 conference, Munich, Germany.

Paper V.

Murtazo Nazarov and Johan Hoffman. On the stability of the dual problem for high Reynolds number flow past a circular cylinder in two dimensions. *Technical report, kth-ctl-4018,* 2011.

The theoretical development, ideas and writing the manuscript of this paper were done in close collaboration between the authors. The author of this thesis performed numerical implementations and was responsible to prepare the manuscript. The author presented a part of this work at the FEF '11 conference, Munich, Germany.

Paper VI.

Murtazo Nazarov and Johan Hoffman. Residual based artificial viscosity for simulation of turbulent compressible flow using adaptive finite element methods. *Technical report, kth-ctl-4019,* 2011.

The theoretical development, ideas and writing the manuscript of this paper were done in close collaboration between the authors. The author of this thesis performed numerical implementations and was responsible to prepare the manuscript.

Acknowledgement

This thesis would have remained incomplete without help of many people. First of all, I would like to thank my supervisor Prof. Johan Hoffman for his guidance, help and encouragement. Thank you for giving me the opportunity to work on such interesting subject and get familiar with the world of finite elements. You always gave me valuable ideas, create a wonderful working environment and encourage me to understand the subject and deal with problems. I would like to thank my second advisor Prof. Anders Szepessy for interesting discussions and valuable comments on my thesis.

Then, I would like to express my gratitude to Prof. Jean-Luc Guermond for his hospitality and letting me join his research group in Texas A&M University. Prof. Bojan Popov is gratefully acknowledged for his collaborative work and insightful ideas. Without Jean-Luc and Bojan Papers I and III would have remained incomplete.

This research is supported by the Swedish Research Council (VR) and the Swedish Foundation for Strategic Research (SSF), which are gratefully acknowledged.

I acknowledge Prof. Jesper Oppelstrup and Prof. Claes Johnson for their interesting and fruitful ideas in finite elements and fluid dynamics.

Prof. Muhamadiev Ergash Mirzoevich and Prof. Naimov Alijon from Vologda State University of Technology, Russia are gratefully acknowledged. Ergash Mirzoevich, when I met you for the first time in Autumn 1997, I could not solve excercise 67 in the Demidovich book. You were not discouraged, to be my mentor and you continuously taught me many things in mathematics and beyond. Having this relationship with you is one of the best achievements I have ever made in my life.

I would like to express my special thanks to the FEniCS community, especially Dr. Anders Logg from Simulla Research Laboratory. I always received valuable replies to all my requests to the mailing list.

Thanks to my collegues at NA/CTL group for creating this pleasant working environment. Especially, I would like to thank Håkon Hoel, Marco Kupiainen, Jelena Popovic, Sara Zahedi and Walter Villanueva for the wonderful time we had together. Thank you Håkon, Kaspar, Jeannette and Walter for your proof readings and comments on this thesis.

My Tajik friends in Stockholm are acknowledged, especially Rustam and Shuhrat and your families for great hospitality the nice time we could spend together.

The special thanks goes to my little family Nargis and Aziz, for their love, understanding, support and encouragement throughout the whole period of this work. My great thanks goes to my family, my sister Maryam, brothers Muzaffar, Mustafo and Mustakim, my mother Muhabbat and father Zoidjon for your continuous love, encouragement and support in my education. You mean everything to me.

Падар ва модари азиз! Ташаккури зиёд барои Шумо, ки ҳамеша маро ба роҳи илму дониш ҳидоят намудед ва новобаста аз сахтии зиндагӣ кӯшиш намудед то маро то ба ин мартаба расонед. Дар симои Шумо боре руҳафтодагиро надидам, ҳамеша пурсабру ботаҳаммул будед. Ин рисола маҳсули заҳмати Шумост, онро бароятон бахшидам.

Оҳиста, аввалин муаллиме буд, ки аллакай то ба мактаб рафтанам бароям хондану ҳисобро омӯзонд ва ҳамеша мегуфт, ки ояндаи ман дар илму маърифат аст. Умедворам бо ин рисола руҳу арвоҳи Ӯ шод хоҳад гашт!

Бо еҳтироми самимӣ,

Murtazo Nazarov
Stockholm, May 26, 2011

Contents

List of Figures

Part I

Introductory Chapters

Chapter 1

Background

1.1 Introduction

The compressible Navier-Stokes equations are a system of conservation laws for *conservation of mass, momentum and energy*. These equations describe the motion of Newtonian flow in fluid dynamics. In the coming chapters we discuss phenomena that arise when the viscosity of the fluid decreases, with shock formation and *turbulence*. Turbulent flow is not well suited for analysis, instead we must use numerical approaches.

In general, problems in science and industry involve complex geometries and shapes. Simulation of flow around cars, airplanes, rackets, wings, birds, and supersonic jets are real examples which can be required from the industry. Therefore, the numerical method should be designed to capture complex geometries. For this reason, we use *finite element methods* because of stability, generality, and applicability to real world problems.

When differential equations are solved numerically, one has to ensure that the method is *efficient* and *reliable*. Efficiency corresponds to solving a problem with small computational cost, and reliability guarantees that the global error can be estimated from the computed solution. This is also one of the main reasons for using finite element methods, since it is mathematically well motivated, with a framework for a posteriori error analysis. Overall, the objective of the thesis is to design and implement a robust stabilized method, and to prove a posteriori error estimates for the compressible Euler equations.

The structure of the thesis is the following: First we give a brief background on conservation laws and the compressible Euler equations in Chapter 1. Then in Chapter 2 we continue our discussion on numerical methods for conservation

laws, where our focus is the Euler equations. Chapter 3 gives information about duality based error estimation for nonlinear problems, and in particular the main theorem for the compressible Euler equations. We discuss different approaches to computational methods for turbulent flows in Chapter 4. We end the thesis by a short conclusion.

For a complete discussion of the stabilized finite element method and error analysis we refer to the attached papers.

This work is a part of the development of the unified continuum mechanics solver *Unicorn* [1], which is based on an adaptive finite element method. The vision of Unicorn is to develop a unified continuum mechanics solver including compressible and incompressible flows, fluid-structure and multiphase problems. Unicorn is part of the *FEniCS applications* and based on components of the *FEniCS project* [2].

1.2 Conservation Laws

The *Initial Value Problem* (IVP) for the n-dimensional *scalar conservation law* is defined as follows:

$$\begin{aligned} \partial_t u + \nabla \cdot \boldsymbol{f}(u) = 0, \quad (\boldsymbol{x}, t) \in \mathbb{R}^n \times \mathbb{R}_+, \\ u(\boldsymbol{x}, 0) = u_0(\boldsymbol{x}), \quad \boldsymbol{x} \in \mathbb{R}^n, \end{aligned} \tag{1.2.1}$$

where $u = u(\boldsymbol{x}, t) : \mathbb{R}^n \times \mathbb{R}_+ \to \mathbb{R}$, $\boldsymbol{f}(u) : \mathbb{R} \to \mathbb{R}^n$ is a given smooth function, and u_0 is initial data which is also given.

We assume that the system (1.2.1) is a *hyperbolic* system of partial differential equations, meaning that the flux Jacobian $\boldsymbol{f}'(u)$ is diagonalizable and has real eigenvalues.

The *Initial Boundary Value Problem* (IBVP) is defined as follows:

$$\begin{aligned} \partial_t u + \nabla \cdot \boldsymbol{f}(u) = 0, \quad \boldsymbol{x} \in \Omega \times \mathbb{R}_+, \\ u(\boldsymbol{x}, 0) = u_0(\boldsymbol{x}), \quad \boldsymbol{x} \in \Omega, \end{aligned} \tag{1.2.2}$$

where $\Omega \subset \mathbb{R}^n$ is a fixed open domain with boundary Γ. The boundary conditions for the IBVP (1.2.2) are based on the characteristics of the flux Jacobian system $\boldsymbol{f}'(u)$. We will later in Chapter 2, Section 2.3.2, discuss the choice of boundary conditions.

1.2.1 Weak Solution

Assume that $\varphi \in \mathcal{C}_0^\infty(\mathbb{R}^n \times \mathbb{R}_+)$ is a smooth test function with compact support. Multiplying this test function to the conservation law (1.2.1) and use

integration by part gives

$$\int_{\mathbb{R}_+}\int_{\mathbb{R}^n} (u\,\partial_t\varphi + \boldsymbol{f}(u)\cdot\nabla\varphi)\,\mathrm{d}\boldsymbol{x}\mathrm{d}t + \int_{\mathbb{R}^n} u_0\varphi(\boldsymbol{x},0)\,\mathrm{d}\boldsymbol{x} = 0. \tag{1.2.3}$$

A function $u(\boldsymbol{x},t)$ is said to be a *weak solution* if it satisfies equation (1.2.3) for all smooth test functions with compact support. The weak formulation (1.2.3) does not include terms with derivatives of the solution u or the flux function $\boldsymbol{f}$.

1.2.2 Viscosity Solution

In general there is no sharp jump in the physical problem even if the conservation law (1.2.1) allows for discontinuities. Instead there is a small diffusive layer over which the solution changes from one value to another. But the layers may be very thin: the thickness of a shock is of the order of the mean free path of the molecules. Therefore, we may replace the above conservation law with a regularized equation

$$\partial_t u + \nabla\cdot\boldsymbol{f}(u) = \epsilon\Delta u, \tag{1.2.4}$$

where ϵ is a small viscosity. The limit when $\epsilon\to 0$ is referred to as a *viscosity solution* to the conservation law.

Viscous regularization makes analysis easier in most cases. However, in the limit when ϵ goes to zero, problems may become more complicated and analysis difficult.

A weak solution u of (1.2.1) is called *admissible in vanishing viscosity sense* if there is a sequence of smooth solutions u^ϵ to

$$\partial_t u^\epsilon + \nabla\cdot\boldsymbol{f}(u^\epsilon) = \epsilon\Delta u^\epsilon, \tag{1.2.5}$$

which converges to u in L^1_{loc} as $\epsilon\to 0+$.

In this thesis we study *the compressible Euler equations*. They play a fundamental role in fluid dynamics describing *inviscid flow*. The Euler equations are obtained from *the Navier-Stokes equations* when the physical viscosity in the system goes to zero.

For the Navier-Stokes equations, the existence[1] of a strong (classical) solution is still not known. A French mathematician, Leray, showed the existence of weak solutions of the incompressible Navier-Stokes equations in three space

[1]This is one of the seven Millennium prizes established by the Clay Mathematics Institute. The prize is US $1,000,000 for a solution or a counter-example.

dimensions [3], but despite of that, the existence of weak solutions for the Euler equations is still unknown. Ladyzhenskaya proved the existence and smoothness of solutions of the Navier-Stokes equations in two space dimensions [4], but this gives no hint in three dimensions, since the main difficulties are absent in two dimensions.

1.2.3 Entropy Solution

Assume that for a solution to (1.2.1), the following inequality holds:

$$\partial_t \eta(u) + \nabla \cdot \boldsymbol{q}(u) \leq 0, \qquad (\boldsymbol{x}, t) \in \mathbb{R}^n \times \mathbb{R}_+, \tag{1.2.6}$$

for a convex function $\eta : \mathbb{R} \to \mathbb{R}$, where $\eta(u)$ is called an *entropy function* and $\boldsymbol{q} : \mathbb{R} \to \mathbb{R}^n$ is the *entropy flux* that is computed from

$$\boldsymbol{q}_i'(u) = \eta'(u)\boldsymbol{f}_i'(u), \quad i = 1, 2, \cdots, n.$$

The weak form of the inequality (1.2.6) is the following: for all non-negative $\varphi \in \mathcal{C}_0^\infty(\mathbb{R}^n \times \mathbb{R}_+)$ we have that

$$\int_{\mathbb{R}_+} \int_{\mathbb{R}^n} \left(\eta(u)\partial_t \varphi + \boldsymbol{q}(u) \cdot \nabla \varphi\right) \mathrm{d}\boldsymbol{x}\mathrm{d}t \geq 0. \tag{1.2.7}$$

A weak solution of (1.2.1) satisfying the entropy inequality (1.2.7) is called an *entropy solution*, or an *entropy admissible solution*.

Clearly, any classical solution of the IVP satisfies the entropy condition (1.2.6), which is seen from multiplication by $\eta'(u)$. In general there are many weak solutions of (1.2.3) that exist for the same initial data. The physically correct solution should satisfy the entropy inequality (1.2.7). One can show that if $u^\epsilon \to u$ in L^1_{loc} as $\epsilon \to 0+$, then u is an entropy solution, see for example [5]. Therefore, the physically correct solution for the conservation law can be obtained as the viscosity solution u^ϵ for vanishing ϵ.

1.2.4 The Riemann Problem and the Rankine Hugoniot Condition

A conservation law together with a piecewise constant initial data, which has a single discontinuity, is called a *Riemann problem*. For the scalar conservation law in 1D, it is defined as:

$$\partial_t u + \frac{\partial}{\partial x} f(u) = 0, \quad u(x, 0) = \begin{cases} u_l, & x < 0, \\ u_r, & x \geq 0. \end{cases} \tag{1.2.8}$$

The initial data has a discontinuity point at $x = 0$ and depending on the values u_l and u_r the problem (1.2.8) has different solutions, such as s*hocks*, *rarefaction waves* and *contact discontinuities*.

If $f'(u_l) > f'(u_r)$, there is a unique entropy solution to the Riemann problem (1.2.8), which is calculated as

$$u(x,t) = \begin{cases} u_l, & x < st, \\ u_r, & x \geq st, \end{cases} \tag{1.2.9}$$

where the constant s is called the *shock speed*. The discontinuity in the solution propagates with the shock speed, satisfying the *Rankine-Huginiot condition*

$$f(u_l) - f(u_r) = s(u_l - u_r). \tag{1.2.10}$$

1.2.5 Example

To understand a family of solutions of the Riemann problem, consider the following initial value problem

$$\partial_t u + \frac{\partial}{\partial x}\left(\frac{u^3}{3}\right) = 0, \quad u_0(x) = \begin{cases} 0, & x < 0, \\ 1, & 0 \leq x < 1, \\ 0, & x \geq 1. \end{cases} \tag{1.2.11}$$

For this problem the shock speed according the Rankine-Hugoniot condition is $s = \frac{1}{3}$. One can easily show that the *characteristics*, $\frac{dx}{dt} = f'(u(x,t))$, for the equation (1.2.11) are straight lines, $x = \xi t + x_0$, $\xi = u^2(x)$, and a solution of (1.2.11) is constant along the characteristics with initial data $u_0(x)$. Then the solution can be found as

$$u(x,t) = \begin{cases} 0, & x < 0, \\ \sqrt{\dfrac{x}{t}}, & 0 \leq x < t, \\ 1, & t \leq x < \dfrac{1}{3}t + 1, \\ 0, & x \geq \dfrac{1}{3}t + 1. \end{cases} \tag{1.2.12}$$

From Figure 1.1 one can see that the characteristic lines do not cross for $x \leq 1$. Between $0 \leq x < t$ a rarefaction wave develops in the solution. The characteristic lines from the region $0 < x < 1$ cross the lines from the region $x \geq 1$, and the *shock line* travels with the shock speed $s = \frac{1}{3}$. Figure 1.2 describes the solution $u(x,t)$ at different times.

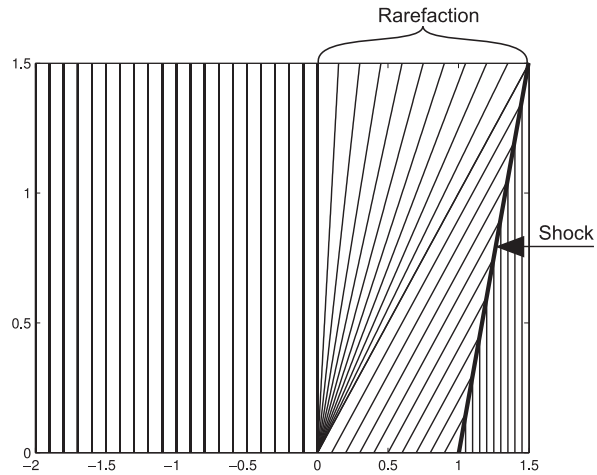

Figure 1.1. The characteristic lines for the equation (1.2.11), (x, t)-plane.

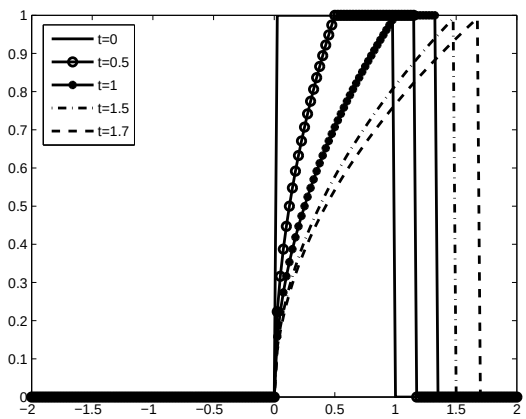

Figure 1.2. Solution of the equation (1.2.11) for different times in the (x, u)-plane.

1.3 The Compressible Euler/Navier-Stokes Equations

A general description of compressible fluids is given by the *compressible Navier-Stokes equations*. The compressible Euler/Navier-Stokes equations play a fundamental role in understanding and simulating compressible gases and fluids and are widely used in science and industry.

The compressible Navier-Stokes equations express conservation of mass, momentum and total energy for a fluid enclosed in a fixed (open) domain Ω in three-dimensional space $\mathbb{R}^3$, with boundary Γ over a time interval $I = [0, \hat{t}\,]$ with initial time zero and final time $\hat{t}$.

The conservation of mass states that the net mass flowing into some control volume must be equal to the rate of increase of total mass in the volume. The conservation of momentum comes directly from Newton's second law, which states that the time rate of change of momentum in a material region is equal to the sum of the forces on that region, or that the sum of forces is equal to mass times acceleration. And finally the conservation of energy states that the total energy in an isolated system remains constant.

We seek the *density* ρ, *momentum* $\boldsymbol{m} = \rho\boldsymbol{u}$, with $\boldsymbol{u} = (\boldsymbol{u}_1, \boldsymbol{u}_2, \boldsymbol{u}_3)$ the *velocity*, and the *total energy* E as functions of $(\boldsymbol{x}, t) \in Q \equiv \Omega \times \Gamma$, where $\boldsymbol{x} = (\boldsymbol{x}_1, \boldsymbol{x}_2, \boldsymbol{x}_3)$ denotes the coordinates in $\mathbb{R}^3$. The equations for $\hat{\boldsymbol{u}} \equiv (\rho, \boldsymbol{m}, E)$ read:

$$\begin{aligned}
\partial_t \rho + \nabla \cdot (\rho \boldsymbol{u}) &= 0 && \text{in } Q,\\
\partial_t \boldsymbol{m} + \nabla \cdot (\boldsymbol{m} \otimes \boldsymbol{u} + \mathbb{I} p) &= \boldsymbol{g} + \nabla \cdot (2\mu\varepsilon(\boldsymbol{u}) + \lambda(\nabla \cdot \boldsymbol{u})\mathbb{I}) && \text{in } Q,\\
\partial_t E + \nabla \cdot (E\boldsymbol{u} + p\boldsymbol{u}) &= \nabla \cdot ((2\mu\varepsilon(\boldsymbol{u}) + \lambda(\nabla \cdot \boldsymbol{u}))\boldsymbol{u} + \kappa \nabla T) && \text{in } Q,\\
\hat{\boldsymbol{u}}(\cdot, 0) &= \hat{\boldsymbol{u}}^0 && \text{in } \Omega,
\end{aligned} \tag{1.3.1}$$

where $p = p(\boldsymbol{x}, t)$ is the *pressure* of the fluid, $\otimes$ denotes the tensor product, $\mathbb{I}$ denotes the identity matrix in $\mathbb{R}^3$, $\partial_t = \partial/\partial_t$ and $\boldsymbol{g} = (\boldsymbol{g}_1, \boldsymbol{g}_2, \boldsymbol{g}_3)$ is a given *volume force* (like gravity) acting on the fluid, $\hat{\boldsymbol{u}}^0 = \hat{\boldsymbol{u}}^0(\boldsymbol{x})$ represents initial conditions,

$$\varepsilon(\boldsymbol{u}) = \frac{1}{2}(\nabla \boldsymbol{u} + \nabla \boldsymbol{u}^T),$$

is the strain rate tensor, and $\kappa \geq 0$ the thermal conduction parameter. The viscosity parameters are assumed to satisfy conditions $\mu > 0$, $\lambda + 2\mu > 0$.

Further, the total energy $E = k + \theta$, where $k = \rho|\boldsymbol{u}|^2/2$ is the *kinetic energy*, with $|\boldsymbol{u}|^2 \equiv \boldsymbol{u}_1^2 + \boldsymbol{u}_2^2 + \boldsymbol{u}_3^2$, and $\theta = \rho T$ is the *internal energy* with T the *temperature* scaled so that $c_v = 1$, where c_v is the heat capacity under constant volume.

For inviscid flow, the viscosity coefficients and thermal conductivity are zero, resulting in absence of viscous forces in equation (1.3.1), which correspond to the compressible Euler equations:

$$\begin{aligned} \partial_t \rho + \nabla \cdot (\rho \boldsymbol{u}) &= 0 && \text{in } Q, \\ \partial_t \boldsymbol{m} + \nabla \cdot (\boldsymbol{m} \otimes \boldsymbol{u} + \mathbb{I} p) &= \boldsymbol{g} && \text{in } Q, \\ \partial_t E + \nabla \cdot (E\boldsymbol{u} + p\boldsymbol{u}) &= 0 && \text{in } Q, \\ \hat{\boldsymbol{u}}(\cdot, 0) &= \hat{\boldsymbol{u}}^0 && \text{in } \Omega. \end{aligned} \tag{1.3.2}$$

For such fluids there is complex behavior, with rarefaction waves, shock waves, and contact discontinuities. Capturing this complex behavior numerically is nontrivial.

The number of unknowns including the pressure is six, but there are only five equations in (1.3.1)-(1.3.2), and so we close the systems with the *state equation* of a *perfect gas*;

$$p = (\gamma - 1)\theta = (\gamma - 1)\rho T = (\gamma - 1)(E - \rho |\boldsymbol{u}|^2/2), \tag{1.3.3}$$

expressing the pressure p as a function of density ρ and temperature T, where $\gamma = c_p$ is the *adiabatic index* with c_p the heat capacity under constant pressure, and $(\gamma - 1)$ is the *gas constant*.

For a perfect gas, the *speed of sound* c is given by $c^2 = \gamma(\gamma - 1)T$, and the *Mach number* is defined as $M = |\boldsymbol{u}|/c$, with $\boldsymbol{u}$ the velocity of the gas. The *total enthalpy* H is given by

$$H = \frac{E}{\rho} + \frac{p}{\rho}. \tag{1.3.4}$$

For the compressible Euler equations the Jacobian matrices $\boldsymbol{f}'(\hat{\boldsymbol{u}}) := \partial_{\hat{\boldsymbol{u}}} \boldsymbol{f}_j(\hat{\boldsymbol{u}})$, $j = 1, 2, 3$, where the fluxes are defined by

$$\boldsymbol{f}(\hat{\boldsymbol{u}}) = \boldsymbol{f}_j(\hat{\boldsymbol{u}}) = \begin{pmatrix} \rho \boldsymbol{u}_j \\ \boldsymbol{m}_i \boldsymbol{u}_j + \partial_{\boldsymbol{x}_i} p \\ (E + p)\boldsymbol{u}_j \end{pmatrix}, \quad i = 1, 2, 3, \tag{1.3.5}$$

are given by

$$\boldsymbol{f}_1'(\hat{\boldsymbol{u}}) = \begin{pmatrix} 0 & 1 & 0 & 0 & 0 \\ -\boldsymbol{u}_1^2 + \frac{1}{2}(\gamma - 1)|\boldsymbol{u}|^2 & (3 - \gamma)\boldsymbol{u}_1 & -(\gamma - 1)\boldsymbol{u}_2 & -(\gamma - 1)\boldsymbol{u}_3 & \gamma - 1 \\ -\boldsymbol{u}_1 \boldsymbol{u}_3 & \boldsymbol{u}_2 & \boldsymbol{u}_1 & 0 & 0 \\ -\boldsymbol{u}_1 \boldsymbol{u}_2 & \boldsymbol{u}_3 & 0 & \boldsymbol{u}_1 & 0 \\ \boldsymbol{u}_1 \frac{1}{2}(\gamma - 1)|\boldsymbol{u}|^2 - H) & H - (\gamma - 1)\boldsymbol{u}_1^2 & -(\gamma - 1)\boldsymbol{u}_1 \boldsymbol{u}_2 & -(\gamma - 1)\boldsymbol{u}_1 \boldsymbol{u}_3 & \gamma \boldsymbol{u}_1 \end{pmatrix}, \tag{1.3.6}$$

$$\boldsymbol{f}_2'(\hat{\boldsymbol{u}}) = \begin{pmatrix} 0 & 0 & 1 & 0 & 0 \\ -\boldsymbol{u}_1\boldsymbol{u}_2 & \boldsymbol{u}_2 & \boldsymbol{u}_1 & 0 & 0 \\ -\boldsymbol{u}_2^2 + \frac{1}{2}(\gamma-1)|\boldsymbol{u}|^2 & -(\gamma-1)\boldsymbol{u}_1 & (3-\gamma)\boldsymbol{u}_2 & -(\gamma-1)\boldsymbol{u}_3 & \gamma-1 \\ -\boldsymbol{u}_2\boldsymbol{u}_3 & 0 & \boldsymbol{u}_3 & \boldsymbol{u}_2 & 0 \\ \boldsymbol{u}_2(\frac{1}{2}(\gamma-1)|\boldsymbol{u}|^2 - H) & -(\gamma-1)\boldsymbol{u}_1\boldsymbol{u}_2 & H-(\gamma-1)\boldsymbol{u}_2^2 & -(\gamma-1)\boldsymbol{u}_2\boldsymbol{u}_3 & \gamma\boldsymbol{u}_2 \end{pmatrix}, \tag{1.3.7}$$

$$\boldsymbol{f}_3'(\hat{\boldsymbol{u}}) = \begin{pmatrix} 0 & 0 & 0 & 1 & 0 \\ -\boldsymbol{u}_1\boldsymbol{u}_3 & \boldsymbol{u}_3 & 0 & \boldsymbol{u}_1 & 0 \\ -\boldsymbol{u}_2\boldsymbol{u}_3 & 0 & \boldsymbol{u}_3 & \boldsymbol{u}_2 & 0 \\ -\boldsymbol{u}_3^2 + \frac{1}{2}(\gamma-1)|\boldsymbol{u}|^2 & -(\gamma-1)\boldsymbol{u}_1 & -(\gamma-1)\boldsymbol{u}_2 & (3-\gamma)\boldsymbol{u}_3 & \gamma-1 \\ \boldsymbol{u}_3(\frac{1}{2}(\gamma-1)|\boldsymbol{u}|^2 - H) & -(\gamma-1)\boldsymbol{u}_1\boldsymbol{u}_3 & H-(\gamma-1)\boldsymbol{u}_2\boldsymbol{u}_3 & -(\gamma-1)\boldsymbol{u}_3^2 & \gamma\boldsymbol{u}_3 \end{pmatrix}. \tag{1.3.8}$$

The eigenvalues of the linearized Euler system, sometimes called characteristic speeds, are: $\boldsymbol{\lambda}_1 = \boldsymbol{\lambda}_2 = \boldsymbol{\lambda}_3 = -\boldsymbol{u}\cdot\boldsymbol{n}$, $\boldsymbol{\lambda}_4 = -\boldsymbol{u}\cdot\boldsymbol{n}+c$, and $\boldsymbol{\lambda}_5 = -\boldsymbol{u}\cdot\boldsymbol{n}-c$, where $\boldsymbol{n} = (\boldsymbol{n}_1, \boldsymbol{n}_2, \boldsymbol{n}_3)$ is an outward unit normal vector to the boundary and c is the speed of sound for an ideal gas. Physically well-posed boundary conditions are imposed according to the characteristic speeds. Incoming waves correspond to characteristics with positive sign while outgoing waves correspond to characteristics with negative sign:

- supersonic inflow: $\boldsymbol{u}$ and $\boldsymbol{n}$ have opposite directions and $|\boldsymbol{u}\cdot\boldsymbol{n}| > c \Rightarrow \boldsymbol{\lambda}_i > 0, \quad i = 1, \cdots, 5$. All 5 characteristics enter to the domain, and 5 boundary conditions need to be imposed;

- supersonic outflow: $\boldsymbol{u}$ and $\boldsymbol{n}$ have the same direction and $|\boldsymbol{u}\cdot\boldsymbol{n}| > c \Rightarrow \boldsymbol{\lambda}_i < 0, \quad i = 1, \cdots, 5$. All characteristics leave the domain, and nothing needs to be imposed;

- subsonic inflow: $\boldsymbol{u}$ and $\boldsymbol{n}$ have opposite directions $|\boldsymbol{u}\cdot\boldsymbol{n}| < c \Rightarrow \boldsymbol{\lambda}_i > 0, \quad i = 1, \cdots, 4, \quad \boldsymbol{\lambda}_5 < 0$. There are 4 characteristic with positive sign, so 4 boundary conditions need to be imposed;

- subsonic outflow: $\boldsymbol{u}$ and $\boldsymbol{n}$ have the same direction and $|\boldsymbol{u}\cdot\boldsymbol{n}| < c \Rightarrow \boldsymbol{\lambda}_i < 0, \quad i = 1, 2, 3, 5, \quad \boldsymbol{\lambda}_4 > 0$. There is one characteristics with positive sign, so one boundary condition needs to be imposed.

For inviscid flow the slip boundary condition $\boldsymbol{u}\cdot\boldsymbol{n} = 0$, requiring the normal velocity to vanish on the boundary, is imposed at the wall boundary. We use the no slip condition $\boldsymbol{u} = 0$ at the wall for the Navier-Stokes equations.

Chapter 2

Stabilized Finite Element Methods for Conservation Laws

2.1 Numerical Methods for Conservation Laws and the Compressible Euler Equations

There are three main numerical approaches to aproximate the compressible Euler equations: *artificial viscosity techniques*, *linear hybridization* and *Godunov's approach*, see [6].

Godunov's approach is based on a Riemann solver and solves the equations exactly at the interior discontinuity interfaces or approximates it using polynomials. In the original Godunov's scheme [7], the solution is approximated by piecewise constant functions, resulting in first order accuracy in space, together with the exact local Riemann solution at the cell interfaces. The piecewise constant functions can be replaced with higher order functions, leading to higher order schemes such as *Monotone Upstream-centered Schemes for Conservation Laws* (MUSCL) [8]. In general, it is hard to use this approach for complex geometries and unstructured grids. Obtaining higher order accurate schemes for unstructured meshes in 3D is not straightforward.

Linear hybridization methods are usually designed in the following way: the regions with a smooth solution is approximated with a high order scheme, while in non smooth regions the scheme is replaced by a lower order scheme which captures steep gradients and discontinuities. Finite difference and finite volume schemes are usually used within this framework. These methods are similar to the artificial viscosity approach, where a small amount of artificial viscosity is added to the scheme in regions near discontinuities. Both need to

find the right regions to give a special treatment.

Artificial viscosity was suggested by Neumann and Richtmyer [9] and has been much developed over the last decades. It regularizes conservation laws by adding extra terms and thereafter the modified equations are solved, see section 1.2.2. Large amount of viscosity can smear out the important characteristics of the solution. For conservation laws, in particular the compressible Euler equations, one has to choose the artificial viscosity in such a way that it reduces oscillations near shocks and discontinuities, but is small in the smooth parts of the domain. One well known approach is to locate shocks by *wavelet coefficients*, proposed by Harten [10]. Wavelet coefficients are used to locate the shock and discontinuity regions, where a small viscosity is then added. However, this approach is restricted to simple rectangular domains.

Later in this chapter we discuss residual based streamline diffusion stabilization and shock capturing methods for finite elements.

2.2 An Overview of Numerical Methods

In this section we discuss some numerical techniques which are used for solving the compressible Euler equations. Among them, the well-known finite difference, finite volume and finite element methods.

2.2.1 Finite Difference and Finite Volume Methods

Finite difference methods are popular with respect to efficiency for certain computational domains. If the computational mesh is structured or equidistant, solution values at the points of the mesh are computed by simple formulas, i.e. keeping the mesh in the computation is not required. For explicit schemes, the solution can be computed at each mesh point without solving a linear system of equations. This makes the program very efficient. Finite difference methods are based on Taylor expansions.

Another method, which is similar to finite difference methods, is the *finite volume method*. The method is based on a volume integral of the partial differential equation where the integrals containing divergences are converted to surface integrals, which are approximated as a flux between volumes. For this method the computational mesh can be both structured or unstructured, and it allows for complex geometry. High accuracy requires information from the neighboring cells. Thus, it is hard to construct a high order accurate scheme with this method, especially in the case of unstructured meshes.

2.2.2 Finite Element Methods

Finite element methods (FEM) are know for their *reliability* and *generality*. FEM is based on the Galerkin method with polynomial basis functions, where the equations are written in *weak form*, by multiplying the equations to a *test function*. FEM is well suited for mathematical analysis, opening for a rigorous error analysis.

FEM can be used in any geometry; it is easy to make a method high order accurate by increasing the order of the basis functions. *Discontinuous Galerkin methods* [11] can be seen as a generalization of finite volume methods.

A disadvantage of the method is the computational efficiency. The method is typically relatively slow on a fixed mesh. However, rigorous error estimation and flexible adaptive mesh refinement can make the method remarkably efficient.

There are Galerkin methods using non polynomial basis functions. The most popular one is the *spectral element method* [12] which is extensively used in fluid dynamics for Direct Numerical Simulations (DNS). Spectral element methods are combinations of spectral methods and finite element methods with special choices of basis functions.

2.3 A Stabilized Finite Element Method

The standard Galerkin finite element method is not stable for convection dominated problems. Instead a mesh-dependent consistent numerical stabilization is added. The development of stabilization methods started in the late 70's. Hughes together with Brooks published the journal paper [13], which summarized the existing stabilized methods. Here they introduced the Streamline Upwind Petrov-Galerkin (SUPG) methods in 1979, see [14], and later Hughes and Tezduyar and their co-workers published a number of papers in this subject, see [15, 16]. For more details about stabilized methods for compressible flow we refer to [17].

Claes Johnson adopted the name *streamline diffusion methods* (SD) and with his coworkers published a series of papers on time dependent problems including advection-diffusion systems, and the Navier-Stokes equations.

The first paper with systematic analysis both mathematically and numerically by Johnson and Nävert appeared already in 1981 in the conference book [18]. Nävert defended his PhD dissertation in 1982 on stabilization of finite element methods [19]. The work by Johnson, Hansbo and Szepessy [20, 21, 22, 23, 24], was mainly focused on stability properties, convergence,

and accuracy of SD for conservation laws including the compressible Euler equations, and the incompressible Navier-Stokes equations.

Another approach of stabilization based on a sub-grid viscosity was proposed by Guermond, where a finite element space is decomposed into a coarse grid space and a fine subgrid space [25, 26], where the stabilization term is only is only active in the subgrid space. This approach was then further developed by Hughes and co-workers as variational multiscale methods [27, 28, 29, 30].

Burman and Hansbo proposed an Edge stabilization technique for convection-diffusion-reaction equations and Stokes problems, which uses least square stabilization of the gradient jumps across element boundaries, see [31, 32].

Recently, a new type of stabilization using a residual of the entropy functional was proposed by Guermond et.al. [33, 34], and efficient implementations of the method, with respect to time discretization and boundary conditions, are studied in [35] in a framework of finite difference/element methods.

2.3.1 Summary of Papers I and II

We start by introducing the following notation: Let $W_h \subset H^1(\Omega)$ be a finite element space consisting of continuous piecewise linear functions on a fixed mesh $\mathcal{T}_h = \{K\}$ of mesh size $h(\boldsymbol{x}) < 1$, with elements K. Here $H^1(\Omega)$ denotes the standard Hilbert space of functions that are square integrable together with their first order derivatives. The scalar product over the finite element mesh $\mathcal{T}_h$ is defined as

$$(\boldsymbol{v}, \boldsymbol{w}) = \sum_{K \in \mathcal{T}_h} \int_K \boldsymbol{v} \cdot \boldsymbol{w} \, \mathrm{d}\boldsymbol{x}.$$

Let $0 = t_0 < t_1 < ... < t_N = \hat{t}$ be a sequence of discrete time steps with time intervals $I_n = (t_{n-1}, t_n]$ and time-step $\Delta t = t_n - t_{n-1}$, and let $\hat{\boldsymbol{u}}_h = (\rho_h, \boldsymbol{m}_h, E_h) \in \boldsymbol{V}_h \equiv W_h \times W_h^3 \times W_h$ be continuous piecewise linear in space.

Entropy Viscosity

In Paper I, we study a stabilization method using entropy viscosity. The entropy viscosity method was originally proposed for a Fourier approximation [33] and was later developed for a finite element formulation in [34]. The idea of the stabilization is the following: we would like to use a Navier-Stokes viscous flux to stabilized the numerical approximation. The artificial dynamic viscosity μ_h, thermal conductivity κ_h, and density viscosity ν_h, are computed as follows:

- For a given approximate solution, $\hat{\boldsymbol{u}}_h(\boldsymbol{x}, t)$, $\boldsymbol{x} \in \Omega, t > 0$, construct an entropy pair η_h and $\boldsymbol{q}_h$ and compute the residual of the entropy inequality:
$$R_\eta(\hat{\boldsymbol{u}}_h) = \partial_t \eta_h(\hat{\boldsymbol{u}}_h) + \nabla \cdot \boldsymbol{q}_h(\hat{\boldsymbol{u}}_h).$$

- Use the above entropy residual to construct the following artificial viscosity for each cell $K \in \mathcal{T}_h$:
$$\mu_E|_K = C_E h_K^2 \|R_\eta(\hat{\boldsymbol{u}}_h)\|_{\infty,K} \|\rho_h\|_{\infty,K} / \|\eta_h - \bar{\eta}_h\|_{L^\infty(\Omega)}$$
where C_E is a tunable parameter, h_K is the smallest edge of the cell K, and $\bar{\eta}_h = \frac{1}{|\Omega|}\int_\Omega \eta_h \mathrm{d}\boldsymbol{x}$ is a normalization parameter. With this normalization we guarantee the dimension of the physical viscosity.

- Compute first order viscosity using a local wave speed:
$$\mu_{\max}|_K = C_{\max} h_K \|\rho_h\|_{\infty,K} \|\boldsymbol{u}_h + \sqrt{\gamma T_h}\|_{\infty,K},$$
where $C_{\max}$ is a tunable parameter, and T_h is an approximation of the temperature.

- Set:
$$\mu_h = \min(\mu_{\max}, \mu_E), \qquad \kappa_h = \frac{\mathcal{P}}{\gamma - 1}\mu_h, \qquad \nu_h = \frac{\mathcal{P}_\rho}{\|\rho_h\|_{\infty,K}}\mu_h,$$
where $\mathcal{P} = \mathcal{O}(1)$ and $\mathcal{P}_\rho = \mathcal{O}(1)$. Our experience is that using $\mathcal{P} \in [0, \frac{1}{4}]$ and $\mathcal{P}_\rho = [0, \frac{1}{5}]$ works well in most cases.

The entropy residual contains a time derivative of the entropy functional. For high accuracy, at least second order backward differentiation needs to be used. That requires to save the solution for two previous time-steps. In Paper I we discuss an alternative way to compute viscosity, where the entropy viscosity is evaluated on the fly in the steps of the Runge-Kutta time-stepping.

In each step of the Runge-Kutta method a linear system involving a mass matrix is solved. Lumping the matrix is a well known technique for fast computation of the mass matrix. Mass lumping consists of approximating the mass matrix M by the diagonal matrix whose entries are the sum of the row entries of M. However, we show computationally that this approach introduces a large dispersion error.

A well-posed boundary condition for conservation laws is based on *characteristic variables* [36, 37]. The implementation of the different boundary conditions for the entropy viscosity finite element method is discussed. We also give a detailed description of the implementation of a slip boundary condition in strong and week forms.

Residual Based Artificial Viscosity

In Paper II we study a simplified case of the streamline diffusion method, were the equations are stabilized by only shock-capturing terms. The shock-capturing terms are computed from the full residual of the Euler equations.

The convergence of the SD method is studied in [38, 39, 40]. Following this work, we prove that the method with only residual based artificial viscosity, or just shock-capturing terms, also converges toward the unique entropy solution. The convergence analysis for a scalar conservation law proceeds by testing that the numerical solution is uniformly bounded, weakly consistent with all entropy inequalities and strongly consistent with the initial data. We show that the backward Euler method with residual based viscosity converges. The same approach for the proof is not possible for explicit schemes. However, we show the performance of explicit schemes in numerical examples for the compressible Euler equations.

2.3.2 Particular Boundary Conditions

There are many boundary conditions used in this thesis. We split the boundary of the domain Ω in: inlet Γ_{inlet}, outlet Γ_{outlet}, and wall Γ_{wall} boundaries. For the complete description of the implementation of boundary conditions in 2D we refer to Paper I. However, in this section we go through the details of the computation of normal and tangent vectors, and a strong implementation of the slip boundary condition in 3D. For completeness, later in this section we describe the characteristic boundary conditions used at the inlet and outlet.

Slip Boundary Conditions

In fluid dynamics, slip boundary conditions are typically used for invisced flows. The slip boundary condition is

$$\boldsymbol{u} \cdot \boldsymbol{n} = 0 \qquad \text{on } \Gamma_{wall} \times I,$$

which means that the normal velocity on the boundary is zero. In other words the pressure is the only nonzero flux on the given boundary $\Gamma_{wall} \times I$.

In our computations, we implement the slip boundary condition strongly. By "strongly" we here mean an implementation of the boundary condition after assembling the stiffness matrix and the load vector, whereas a "weak" implementation involves adding boundary integrals to the variational formulation. The row of the matrix and load vector corresponding to a boundary vertex is found and replaced by a new row according to the boundary condition.

The idea is as follows: Initially, the test function $\boldsymbol{v}$ is expressed in the Cartesian standard basis $(\boldsymbol{e}_1, \boldsymbol{e}_2, \boldsymbol{e}_3)$. Now, the test function is mapped locally to normal-tangent coordinates with the basis $(\boldsymbol{n}, \boldsymbol{\tau}_1, \boldsymbol{\tau}_2)$, where $\boldsymbol{n} = (\boldsymbol{n}_1, \boldsymbol{n}_2, \boldsymbol{n}_3)$ is the normal, and $\boldsymbol{\tau}_1 = (\boldsymbol{\tau}_{11}, \boldsymbol{\tau}_{12}, \boldsymbol{\tau}_{13})$, $\boldsymbol{\tau}_2 = (\boldsymbol{\tau}_{21}, \boldsymbol{\tau}_{22}, \boldsymbol{\tau}_{23})$ are tangents to each node on the boundary. This allows us to let the normal direction to be constrained and the tangent directions be free:

$$\boldsymbol{v} = (\boldsymbol{v} \cdot \boldsymbol{n})\boldsymbol{n} + (\boldsymbol{v} \cdot \boldsymbol{\tau}_1)\boldsymbol{\tau}_1 + (\boldsymbol{v} \cdot \boldsymbol{\tau}_2)\boldsymbol{\tau}_2.$$

For the matrix and vector this means that the rows corresponding to the boundary nodes need to be multiplied with $\boldsymbol{n}, \boldsymbol{\tau}_1, \boldsymbol{\tau}_2$, respectively, added together, and then the normal velocity should be put 0.

In the 2D case there is only one tangential vector so that the new basis is $(\boldsymbol{n}, \boldsymbol{\tau})$. Here we present the implementation for 3D, but modification to 2D is straight forward.

We split the boundary vertices of the computational domain into three types, see Fig. 2.1:

- type S_1 - where a vertex is on a surface,
- type S_2 - where a vertex is on a edge,
- type S_3 - where a vertex is on a corner.

Normals and Tangential Vectors

The discussion below is for convex boundaries, but is valid for concave boundaries as well. For the first type, S_1, we follow the algorithm in [41] to find the normal and tangential vectors. Here the tangential vectors are calculated for a given normal vector $\boldsymbol{n} = (\boldsymbol{n}_1, \boldsymbol{n}_2, \boldsymbol{n}_3)$, with the normal vector given for each facet of an element.

We define facets to belong to the same surface if the angle, α, between the facet normals are less in absolute value than $\alpha_{max} > 0$. In this thesis we choose $\alpha_{max} = \frac{\pi}{6}$. For each surface a normal to a vertex is calculated as a weighted average of all the facet normals which contain the vertex with the weight being the area of each facet.

We define the vertex to belong to an *edge*, or type S_2, if the vertex belongs to two surfaces. In this case, we take the normal from the first surface as vector $\boldsymbol{n}$; and the normal from the second surface as $\boldsymbol{\tau}_1$. The last vector $\boldsymbol{\tau}_2$ is then a cross product of $\boldsymbol{n}$ and $\boldsymbol{\tau}_1$, $\boldsymbol{\tau}_2 = \boldsymbol{n} \times \boldsymbol{\tau}_1$. When $\alpha = \frac{\pi}{2}$ normals are perpendicular. But in general vectors $\boldsymbol{n}$ and $\boldsymbol{\tau}_1$ are not necessarily perpendicular, see Fig. 2.2.

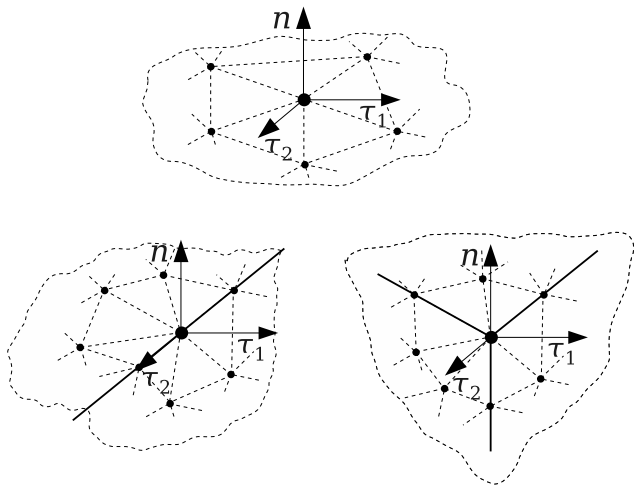

Figure 2.1. The possible types of the boundary, S_1 (upper), S_2 (lower left) and S_3 (lower right).

The third case is a vertex which belongs to more than two surfaces. Again the angle between normals on the surfaces, α, is checked. If there are more than two surfaces we say the vertex belongs to a *corner*, or type S_3.

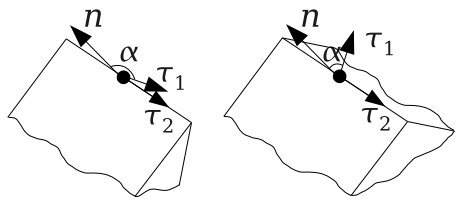

Figure 2.2. Some different types of edges.

Implementation

Let us assume that the degrees of freedom (d.o.f.) are enumerated as follows: the density d.o.f. are enumerated from 1 to N, the first Cartesian component d.o.f. of the momentum are enumerated from $1+N$ to $2N$, the second Cartesian component d.o.f. are enumerated from $1+2N$ to $3N$, the third Cartesian component d.o.f. are enumerated from $1+3N$ to $4N$, and the total

energy d.o.f. are enumerated from $1+4N$ to $5N$. Assume that no boundary condition is enforced, where we end up solving the linear system of equations $\mathbf{A}\hat{\boldsymbol{u}}(K_l) = \mathbf{b}$, where K_l denotes the set consisting of all d.o.f., $\mathbf{A}$ is a $(5N, 5N)$ stiffness matrix and $\mathbf{b}$ a load vector. Let $i \in K_l$ be a boundary node where we want to enforce the slip boundary condition:

$$\begin{pmatrix} \cdots & \cdots & \cdots & \cdots & \cdots & \cdots & \cdots \\ \cdots & a_{i+N,i+N} & \cdots & a_{i+N,i+2N} & \cdots & a_{i+N,i+3N} & \cdots \\ \cdots & \cdots & \cdots & \cdots & \cdots & \cdots & \cdots \\ \cdots & a_{i+2N,i+N} & \cdots & a_{i+2N,i+2N} & \cdots & a_{i+2N,i+3N} & \cdots \\ \cdots & \cdots & \cdots & \cdots & \cdots & \cdots & \cdots \\ \cdots & a_{i+3N,i+N} & \cdots & a_{i+3N,i+2N} & \cdots & a_{i+3N,i+3N} & \cdots \\ \cdots & \cdots & \cdots & \cdots & \cdots & \cdots & \cdots \end{pmatrix} \cdot \begin{pmatrix} \cdots \\ \rho \boldsymbol{u}_i^1 \\ \cdots \\ \rho \boldsymbol{u}_i^2 \\ \cdots \\ \rho \boldsymbol{u}_i^3 \\ \cdots \end{pmatrix} = \begin{pmatrix} \cdots \\ l_{i+N} \\ \cdots \\ l_{i+2N} \\ \cdots \\ l_{i+3N} \\ \cdots \end{pmatrix}$$

Let us discuss the implementation of the slip boundary condition for each part separately.

(a) type S_1. After a local coordinate mapping from the Cartesian to the normal- tangent coordinate system and putting the normal velocity to zero, the matrix $\mathbf{A}$ takes the following form.

$$\begin{pmatrix} \cdots & \cdots & \cdots & \cdots & \cdots & \cdots & \cdots \\ 0 & \boldsymbol{n}_1 & 0 & \boldsymbol{n}_2 & 0 & \boldsymbol{n}_3 & 0 \\ \cdots & \cdots & \cdots & \cdots & \cdots & \cdots & \cdots \\ \cdots & a'_{i+2N,i+N} & \cdots & a'_{i+2N,i+2N} & \cdots & a'_{i+2N,i+3N} & \cdots \\ \cdots & \cdots & \cdots & \cdots & \cdots & \cdots & \cdots \\ \cdots & a''_{i+3N,i+N} & \cdots & a''_{i+3N,i+2N} & \cdots & a''_{i+3N,i+3N} & \cdots \\ \cdots & \cdots & \cdots & \cdots & \cdots & \cdots & \cdots \end{pmatrix} \cdot \begin{pmatrix} \cdots \\ \rho \boldsymbol{u}_i^1 \\ \cdots \\ \rho \boldsymbol{u}_i^2 \\ \cdots \\ \rho \boldsymbol{u}_i^3 \\ \cdots \end{pmatrix} = \begin{pmatrix} \cdots \\ 0 \\ \cdots \\ l'_{i+2N} \\ \cdots \\ l''_{i+3N} \\ \cdots \end{pmatrix}$$

where

$$\begin{aligned} a'_{i+2N,j} &= a_{i+N,j}\boldsymbol{\tau}_{11} + a_{i+2N,j}\boldsymbol{\tau}_{12} + a_{i+3N,j}\boldsymbol{\tau}_{13}, \quad j = 1, 2, \cdots, 5N, \\ l'_{i+2N} &= l_{i+N}\boldsymbol{\tau}_{11} + l_{i+2N}\boldsymbol{\tau}_{12} + l_{i+3N}\boldsymbol{\tau}_{13}, \end{aligned}$$

and

$$\begin{aligned} a''_{i+3N,j} &= a_{i+N,j}\boldsymbol{\tau}_{21} + a_{i+2N,j}\boldsymbol{\tau}_{22} + a_{i+3N,j}\boldsymbol{\tau}_{23}, \quad j = 1, 2, \cdots, 5N, \\ l''_{i+3N} &= l_{i+N}\boldsymbol{\tau}_{21} + l_{i+2N}\boldsymbol{\tau}_{22} + l_{i+3N}\boldsymbol{\tau}_{23}. \end{aligned}$$

Note that the mapping is done locally only for the vertex on the boundary, which means the rest of the rows remain the same.

(b) type S_2. In this case, there are two normals by the above construction, n and $\boldsymbol{\tau}_1$. Velocity in these directions is constrained. The velocity in the third direction, $\boldsymbol{\tau}_2$, is free. The linear system takes the following form:

$$\begin{pmatrix} \cdots & \cdots & \cdots & \cdots & \cdots & \cdots & \cdots \\ 0 & \boldsymbol{n}_1 & 0 & \boldsymbol{n}_2 & 0 & \boldsymbol{n}_3 & 0 \\ \cdots & \cdots & \cdots & \cdots & \cdots & \cdots & \cdots \\ 0 & \boldsymbol{\tau}_{11} & 0 & \boldsymbol{\tau}_{12} & 0 & \boldsymbol{\tau}_{13} & 0 \\ \cdots & \cdots & \cdots & \cdots & \cdots & \cdots & \cdots \\ \cdots & a''_{i+3N,i+N} & \cdots & a''_{i+3N,i+2N} & \cdots & a''_{i+3N,i+3N} & \cdots \\ \cdots & \cdots & \cdots & \cdots & \cdots & \cdots & \cdots \end{pmatrix} \cdot \begin{pmatrix} \cdots \\ \rho \boldsymbol{u}_i^1 \\ \cdots \\ \rho \boldsymbol{u}_i^2 \\ \cdots \\ \rho \boldsymbol{u}_i^3 \\ \cdots \end{pmatrix} = \begin{pmatrix} \cdots \\ 0 \\ \cdots \\ 0 \\ \cdots \\ l''_{i+3N} \\ \cdots \end{pmatrix}$$

(c) type S_3. For a corner, the velocity in all directions is constrained. Therefore, it is the same as applying a no-slip or zero velocity boundary condition for this vertex. Meaning here that the row is replaced by an identity vector and the right hand side is set to zero.

To ensure good conditioning of the matrix the rows are finally rearranged to have the largest matrix elements on the diagonal.

Inlet/outlet boundary conditions

Imposing numerical and physical boundary conditions highly depends on the direction of the propagating waves. The eigenvalues of the Euler system, characteristics speeds, are found as follows: $\boldsymbol{\lambda}_1 = \boldsymbol{\lambda}_2 = -\boldsymbol{u}\cdot\boldsymbol{n}$, $\boldsymbol{\lambda}_3 = -\boldsymbol{u}\cdot\boldsymbol{n}+c$, and $\boldsymbol{\lambda}_4 = -\boldsymbol{u}\cdot\boldsymbol{n}-c$, where c is the speed of sound for an ideal gas. The normal and tangent vectors are defined above.

Following Löhner [42] we apply characteristic based boundary conditions at inlet Γ_{inlet} and outlet Γ_{outlet}. Characteristic variables of the one-dimensional Euler equations are found locally in each boundary cells, then they are fixed according to the incoming waves for non-reflecting boundary conditions. For the supersonic case all characteristics enter the computational domain at the inflow, whereas they leave the domain at the outflow. In this case Dirichlet boundary conditions are imposed for all variables at the inlet, but nothing is imposed at the outflow. One boundary condition, typically for pressure, is imposed at subsonic outlet.

For the detailed discussion of these type of boundary conditions, see Paper I.

2.3.3 Numerical Examples

We consider Mach 3 flow in a wind tunnel with a step. This is a well known benchmark used for testing new methods since [6]. Here we consider the two dimensional case.

The wind tunnel of length 3 and height 1 contains a step with height 0.2, situated at a distance 0.6 from the inflow. The initial data for the problem is $\rho = 1.4, \boldsymbol{m} = (4.2, 0), E = 8.8$. The flow is influenced by the numerical error appearing from the neighborhood of the singular corner, where this affect can be seen in the bottom Mach stem. Woodward and Colella [6] proposed to apply a special kind of boundary condition for the points close to the corner, to avoid the effect from the singularity. Another approach could be to round off the nonphysically sharp corner and allow adaptive mesh refinement to

follow the smooth structure of the rounded corner. We round off the corner with a relatively small fixed curvature. It decreases the numerical error at the corner up to a certain level. In the case of supersonic flow all characteristics of the Euler equations go to the right, therefore no physical boundary conditions are needed at the outflow. A slip or reflecting boundary condition is applied on the channel walls. Usually, for numerical tests this simulation is done until time $t = 4$.

The residual based artificial viscosity as in Paper II is used for the stabilization. We use three different meshes: a coarse mesh with 6939 nodes, 13512 cells and $h = 0.025$; a medium with 27389 nodes, 54048 cells and $h = 0.0125$; and a fine with 153864 nodes, 306156 cells and $h = 0.00763$.

Figure 2.3 shows the mesh for the medium mesh close to the corner. This technique removes any numerical error which appears when the corner is not rounded. The mesh is relatively finer in the close neighborhood of the corner. We present our result in Figures 2.4, 2.5 and 2.6. We plot density and pressure from the coarse, medium and fine meshes in Figures 2.4 and 2.5. We observe that even for the coarsest mesh the method captures the right locations of the strong shock and a contact discontinuity is clearly visible. The contact discontinuity is resolved well in the finest mesh. The medium mesh corresponds approximately to the same mesh of size 80×240 which is used in [6]. The approximation obtained by the residual based viscosity used in this thesis is comparable with the high order finite difference schemes used in [6].

The magnitude of the residual based artificial viscosity is plotted in Figure 2.6 for three meshes. We see that the viscosity is active mostly at the shocks, while it is very small in the smooth region. The viscosity gets more localized as the mesh is refined. We observe that the viscosity is small in the region where a contact discontinuity develops.

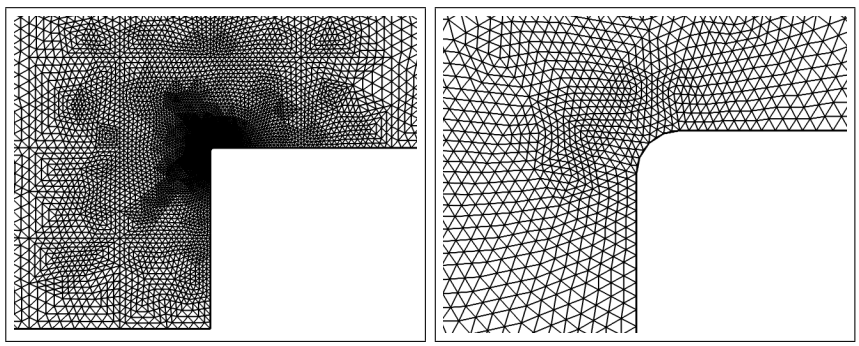

Figure 2.3. Wind-tunnel with forward-facing step: the medium size mesh with $h = 0.0125$. Triangulation close to the step at the left, and zoom of the corner at the right. The mesh size at the curvature is $h = 0.00072$.

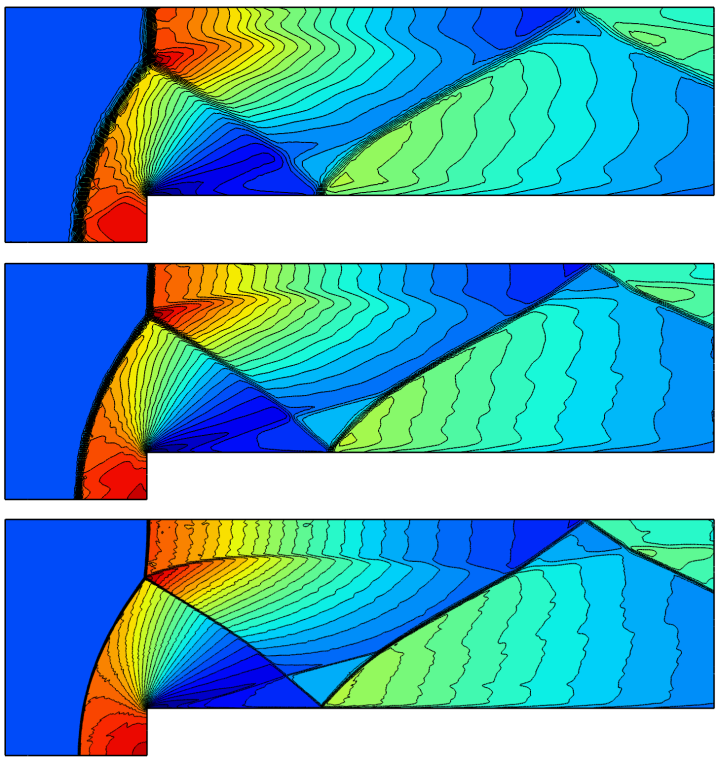

Figure 2.4. Wind-tunnel with forward-facing step: Colormap and 30 contours of density for the coarsest mesh, $h = 0.025$, $0.1775 \leq \rho \leq 6.0906$, at the top, medium mesh, $h = 0.0125$, $0.1245 \leq \rho \leq 6.2552$, at the middle, and finest mesh, $h = 0.00763$, $0.1245 \leq \rho \leq 6.2552$, at the bottom.

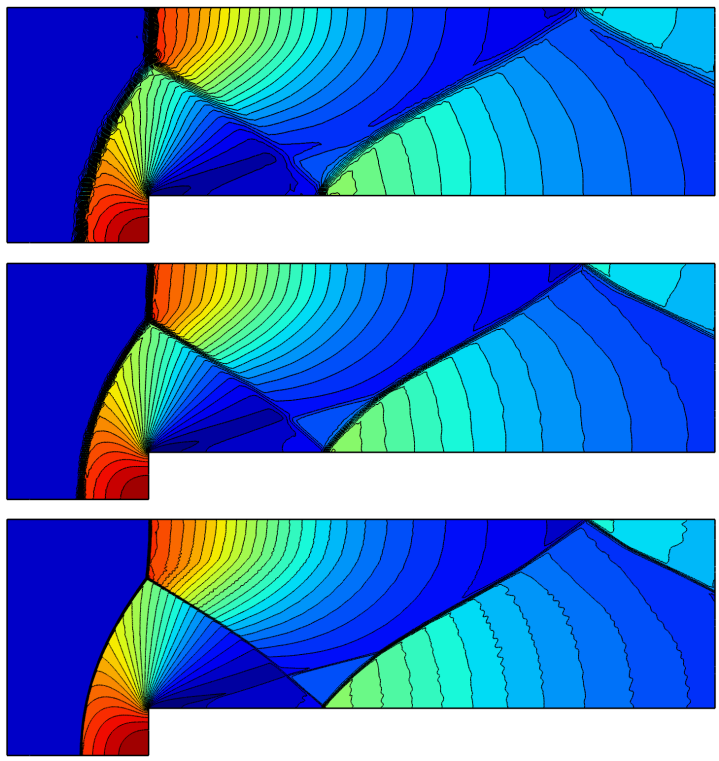

Figure 2.5. Wind-tunnel with forward-facing step: Colormap and 30 contours of pressure for the coarsest mesh, $h = 0.025$, $0.24 \leq p \leq 11.94$, at the top, medium mesh, $h = 0.0125$, $0.1536 \leq p \leq 11.961$, at the middle, and finest mesh, $h = 0.00763$, $0.1331 \leq p \leq 12,1118$, at the bottom.

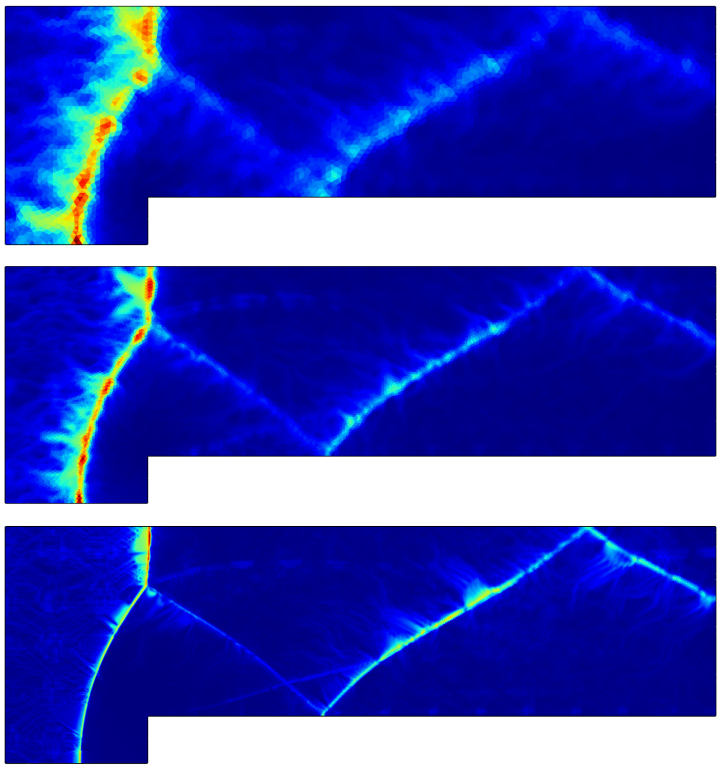

Figure 2.6. Wind-tunnel with forward-facing step: Colormap of residual based artificial viscosity, Paper II: coarsest mesh, $h = 0.025$, $1.03e-4 \leq \mu \leq 0.0657$, at the top, medium mesh, $h = 0.0125$, $2.77e-5 \leq \mu \leq 0.0582$, at the middle, and finest mesh, $h = 0.00763$, $1.18e-5 \leq \mu \leq 0.022$, at the bottom.

Chapter 3

Error analysis for finite element methods

An a priori error estimate shows that for a class of problems, a finite element method produces the best approximation $\boldsymbol{U}$ in the finite element space $\boldsymbol{V}_h$ of the exact solution $\boldsymbol{u}$, see e.g. [43, 44].

In a posteriori error analysis, only knowledge of the computed solution is required. This means that the solution $\boldsymbol{U}$ is computed, and then the error is estimated using this solution. Once the bound of the error is estimated in the appropriate norm, it is possible to improve the approximation in order to reduce the error which makes the method efficient and reliable. The idea of using duality arguments in a posteriori error estimation was first studied by Babuška and Miller for elliptic model problems [45, 46]. A more general framework for a systematic approach to a posteriori error estimation was developed by Eriksson and Johnson, Becker and Rannacher, with co-workers, [43, 47, 48, 49, 50, 51, 52, 53, 54, 55, 56].

In most applications we are interested in obtaining an estimate of the error in some *quantity of interest* or *output*, rather than, say, the L_2 norm of the error. The quantity of interest can be fluid forces such as drag and lift, stresses and fluxes. For more information, see e.g. [44]. This approach identifies a region in the computational domain, which must be refined to improve the accuracy in the quantity of interest. The improvement is then done by so called *h-p-adaptivity*, where h refers to splitting the cell (triangles, tetrahedrons) into several smaller cells, and p refers to increasing the order of a polynomial degree locally. Babuška and his co-workers show that by suitably identifying regions with high error and using h-p-adaptivity the finite element methods converge exponentially, see e.g. [57, 58]. In this thesis we focus on h-adaptivity.

3.1 A posteriori error estimation for the compressible Euler equations

For systems of conservation laws, a posteriori error analysis has been investigated by Johnson, Szepessy and Hansbo [59, 60], and the stationary compressible Euler equations in 2D have been studied by Hartmann, Huston and Süli, and Larson and Barth using adaptive discontinuous Galerkin methods [61, 62, 63, 64]. Burman studied a posteriori error estimation for the time dependent compressible Euler equations in 2D [65].

In this thesis we present a posteriori error estimates for the compressible Euler equations in three space dimensions, where we formulate the Euler equations (1.3.2) in terms of density, velocity and pressure. These variables are independent of each other, resulting in a simplified derivation of the a posteriori error estimate. For details we refer to Paper III of the thesis, where we show the derivation of the dual problem for the compressible Euler equations and we prove an a posteriori error estimate [66].

To understand the essence of a posteriori error analysis for nonlinear problems, including the compressible Euler equations, consider the following nonlinear equation in a finite n-dimensional space:

$$\mathcal{F}(\boldsymbol{u}) = \boldsymbol{b}, \tag{3.1.1}$$

where $\mathcal{F} : \mathbb{R}^n \mapsto \mathbb{R}^n$, $\boldsymbol{u} \in \mathbb{R}^n$.

The *residual* of a computed approximate solution $\boldsymbol{U} \in \mathbb{R}^n$ is defined as

$$\mathcal{R}(\boldsymbol{U}) = \mathcal{F}(\boldsymbol{U}) - \boldsymbol{b}, \tag{3.1.2}$$

or we can write

$$-\mathcal{R}(\boldsymbol{U}) = \mathcal{F}(\boldsymbol{u}) - \mathcal{F}(\boldsymbol{U}). \tag{3.1.3}$$

To derive a relation between the residual $R(\boldsymbol{U})$ and the error $\boldsymbol{e} = \boldsymbol{u} - \boldsymbol{U}$,we insert $\boldsymbol{u} = \boldsymbol{U} + \boldsymbol{e}$ in (3.1.1) and Taylor expand about $\boldsymbol{U}$ to get

$$\begin{aligned} \mathcal{F}(\boldsymbol{U} + \boldsymbol{e}) = \boldsymbol{b} \quad &\Rightarrow \\ \mathcal{F}(\boldsymbol{U}) + \mathcal{F}'(\boldsymbol{U})\boldsymbol{e} + \mathcal{O}(\boldsymbol{e}^2) = \boldsymbol{b} \quad &\Rightarrow \\ \mathcal{F}'(\boldsymbol{U})\boldsymbol{e} + \mathcal{O}(\boldsymbol{e}^2) = -(\mathcal{F}(\boldsymbol{U}) - \boldsymbol{b}) \quad &\Rightarrow \\ \mathcal{F}'(\boldsymbol{U})\boldsymbol{e} + \mathcal{O}(\boldsymbol{e}^2) = -\mathcal{R}(\boldsymbol{U}) & \end{aligned} \tag{3.1.4}$$

where $\mathcal{F}'(\boldsymbol{U})$ is a Jacobian matrix. We drop the remaining terms which is of order $\mathcal{O}(\boldsymbol{e}^2)$, to write the relation between residual and error as

$$\mathcal{F}'(\boldsymbol{U})\boldsymbol{e} \approx -\mathcal{R}(\boldsymbol{U}). \tag{3.1.5}$$

The adjoint problem is used to determine the effect on a quantity of interest of the accumulation of errors.

With the notation $\mathcal{A}(\boldsymbol{e}) = \mathcal{F}'(\boldsymbol{U})\boldsymbol{e}$ we use the definition of an adjoint operator and multiply the left hand side by $\boldsymbol{\phi}$ and integrate by parts

$$(\mathcal{A}(\boldsymbol{e}), \boldsymbol{\phi}) = (\mathcal{F}'(\boldsymbol{U})\boldsymbol{e}, \boldsymbol{\phi}) = (\boldsymbol{e}, [\mathcal{F}'(\boldsymbol{U})]^T\boldsymbol{\phi}) = (\boldsymbol{e}, \mathcal{A}^*(\boldsymbol{\phi})), \tag{3.1.6}$$

where $\mathcal{A}^*$ is an adjoint operator of $\mathcal{A}$. Using the adjoint operator $\mathcal{A}^*$, we define the following *dual problem* for the variable ϕ: find $\phi \in \mathbb{R}^n$ such that

$$\mathcal{A}^*(\boldsymbol{\phi}) = \boldsymbol{\psi}, \tag{3.1.7}$$

where $\boldsymbol{\psi} \in \mathbb{R}^n$ defines *a linear target functional* $\mathcal{M}(\boldsymbol{u})$ of the problem by $\mathcal{M}(\boldsymbol{u}) = (\boldsymbol{u}, \boldsymbol{\psi})$. The functional $\mathcal{M}(\boldsymbol{u})$ is sometime called as *a quantity of interest*. The quantity $\mathcal{M}(\boldsymbol{u})$ can be the error at some point, the error in an average over some subset of the computational domain, or the error in some norm.

The following lemma is an error representation formula:

Lemma 3.1.1. *The error in the target functional* $\mathcal{M}(\boldsymbol{u}) - \mathcal{M}(\boldsymbol{U}) = \mathcal{M}(\boldsymbol{e})$ *has the following relation to the residual* $\mathcal{R}(\boldsymbol{U})$*, and dual solution* $\boldsymbol{\phi}$

$$\mathcal{M}(\boldsymbol{e}) \approx (-\mathcal{R}(\boldsymbol{U}), \boldsymbol{\phi}). \tag{3.1.8}$$

Proof. Using the definition of the adjoint operator, (3.1.6), and the dual problem (3.1.7), we have the following error representation for the quantity of interest:

$$\mathcal{M}(\boldsymbol{u}) - \mathcal{M}(\boldsymbol{U}) = \mathcal{M}(\boldsymbol{e}) = (\boldsymbol{e}, \boldsymbol{\psi}) = (\boldsymbol{e}, \mathcal{A}^*(\boldsymbol{\phi})) \approx (-\mathcal{R}(\boldsymbol{U}), \boldsymbol{\phi}). \tag{3.1.9}$$

□

3.2 Summary of Papers III, IV and V

We show duality based a posteriori error estimations in Papers III, IV and V.

In Paper III we prove an a posteriori error estimate in terms of the primitive variables of the compressible Euler equations. We give a detailed analysis of the linearization of the system and derivation of the adjoint problem. A simplified streamline diffusion method with continuous piecewise linear functions in space and time is used to approximate the primal problem. The dual problem is stabilized by a first order artificial viscosity. The time discretization corresponds to the implicit Crank-Nicholson method for both the primal

and dual problems. A number of examples are performed in 2D and 3D. This paper can be seen as an extension of previous work on adaptive finite element methods for turbulent incompressible flow [67, 68, 69, 70].

In Paper IV we prove a posteriori error estimates using conservation variables. Both the primal and dual problems are solved in time by explicit Runge-Kutta methods. The entropy based viscosity is used for the primal, and a residual based stabilization is used for the dual problem. Flow around a Naca 0012 airfoil is studied for various Mach numbers and target functionals. The results are validated and discussed with respect to reference results.

We prove the following estimates: Assume $\hat{\boldsymbol{u}}_h = (\rho_h, \boldsymbol{m}_h, E_h)$ is a finite element approximation and $\hat{\boldsymbol{u}} = (\rho, \boldsymbol{m}, E)$ is the exact solution, and $\hat{\boldsymbol{\phi}} = (\phi_\rho, \boldsymbol{\phi}_{\boldsymbol{m}}, \phi_E)$ is the exact solution of the linearized dual problem of the Euler equations.

Then the following theorem is *an a posteriori error estimate for the compressible Euler equations.*

Theorem 3.2.1. *The error, $\mathcal{M}(\hat{\boldsymbol{u}}) - \mathcal{M}(\hat{\boldsymbol{u}}_h)$ satisfies the following inequality*

$$\begin{aligned} |\mathcal{M}(\hat{\boldsymbol{u}}) - \mathcal{M}(\hat{\boldsymbol{u}}_h)| \leq & \int_I \sum_{K\in\mathcal{T}_n} C_h h_K |\mathcal{R}(\hat{\boldsymbol{u}}_h)|_K \cdot |D\hat{\boldsymbol{\phi}}|_K \\ & + \int_I \sum_{K\in\mathcal{T}_n} |Vis(\hat{\boldsymbol{u}}; \pi_h\hat{\boldsymbol{\phi}})_K| \mathrm{d}t + h.o.t., \end{aligned} \tag{3.2.1}$$

where h_K is the meshsize, h.o.t. is higher order terms, $\mathcal{T}_h = \{K\}$ is a fixed mesh with mesh size $h_K(\boldsymbol{x}) < 1$ and elements K, where, for $\boldsymbol{w} \in \boldsymbol{V}_h$, $Vis(\hat{\boldsymbol{u}}; \boldsymbol{w})_K$ is stabilization terms in the finite element discretization.

In our computation we use $C_h = \frac{1}{8}$, which can be motivated by a simple analysis on reference elements. Further, we denote by $\mathcal{S} = \int_I |D\hat{\boldsymbol{\phi}}|_K \mathrm{d}t$ a stability factor of the dual problem. The stability factor measures output sensitivity of the quantity of interest with respect to numerical errors. The a posteriori error estimate is expressed in terms of computed solutions of the primal and dual problems. If the quantity $|h_K\mathcal{R}(\hat{\boldsymbol{u}}_h)|$ decreases by mesh refinement and the stability weight $|D\hat{\boldsymbol{\phi}}|_K$ is of moderate size, then the error in the target functional is *computable*.

Paper V discusses stability issues of the dual solution for a 2D flow around a circular cylinder for high Reynolds numbers for different Mach numbers. We test the following Mach numbers: $M = 0.2, 0.4, 0.6, 0.8, 1.4, 2.0$, corresponding to subsonic, transonic and supersonic inlets. We observe that for these Mach numbers the dual solution of a drag functional blows up in the numerical

computations, and we discuss the fact that such blowup for 3D computation of incompressible Navier-Stokes equations is not observed.

3.3 An Adaptive Algorithm

Once the a posteriori error estimate is obtained, the next step is to use the error indicator in (3.2.1) to improve the numerical approximation. In the simplest *adaptive algorithms*, the mesh $\mathcal{T}_h$ remains constant until the final time $\hat{t}$. For the fixed mesh, the primal problem is solved forward and the dual problem is solved backward in time. Then the mesh is refined/coarsened according to the error indicator. Then the whole cycle is repeated until some criteria is satisfied:

Algorithm 3.3.1. *Given some tolerance* TOL *and initial coarse mesh* $\mathcal{T}_h^0$. *Starting with time* $k = 0$, *do the following adaptive loop:*

1. *Compute the finite element approximation* $\hat{\mathbf{u}}_h$ *on the current mesh* $\mathcal{T}_h^k$.
2. *Compute the approximate dual solution,* $\hat{\boldsymbol{\phi}}_h$, *on the same mesh.*
3. *Compute the error indicator defined in (3.2.1), if* $|\mathcal{M}(\hat{\mathbf{u}}) - \mathcal{M}(\hat{\mathbf{u}}_h)| <$ TOL, *then* STOP.
4. *Refine elements in* $\mathcal{T}_h^k$ *with the largest error indicator to get mesh* $\mathcal{T}_h^{k+1}$.
5. *Set* $k = k + 1$ *and go to 1.*

3.4 Numerical Examples

Here we consider subsonic flow past a Naca 0012 airfoil. The equation of the upper and lower surfaces of the Naca 0012 airfoil is defined as the follows:

$$y(x) = \pm\frac{t}{0.2}l\left(0.2969\sqrt{\frac{x}{l}} - 0.126\left(\frac{x}{l}\right) - 0.3516\left(\frac{x}{l}\right)^2 + 0.2843\left(\frac{x}{l}\right)^3 - 0.1015\left(\frac{x}{l}\right)^4\right), \tag{3.4.1}$$

where $x \in [0, l]$, $l \approx 1.00893$ is the chord length and $t = 12 \cdot 0.01 \cdot l$ is a maximum thickness of the airfoil, see Figure 3.1.

We solve the primal and dual problem of the compressible Euler equations for drag and lift as a target functionals. The entropy viscosity method presented in Paper I is used to solve the primal problem. The parameters used for the entropy viscosity stabilization in the computation of the primal problem are: CFL number 0.5, Prandtl numbers $\mathcal{P} = 0.1$ and $\mathcal{P}_\rho = 0.1$, the parameter

Figure 3.1. Naca 0012 airfoil: geometry.

of the first order viscosity is $C_{max} = 0.2$ and that of the entropy viscosity is $C_E = 1.0$. For the dual problem we use a residual based viscosity stabilization with: CFL number 0.5, $C_{max} = 0.1$, and $C_E = 0.25$. The initial condition of the problem is $\rho = 1.4$, $p = 1$, $u = M = 0.8$ and the angle of attack is chosen to be $\alpha = 1.25$. The coarsest mesh consists of 1114 nodes and 2136 cells. The averaging window of the computation of the target functionals is chosen as $t \in [80, 120]$, meaning that the primal problem is solved up to $t = 120$, and thereafter the adjoint problem is solved backward in time back to $t = 80$. The total error is then estimated, 10% of cells with the largest error contributions are refined, and the process is then repeated.

This problem is known for it's stationary solution consisting of shocks on both upper and lower surfaces of the airfoil, see for example [71, 72]. We present the results of the problem in the following figures. Figure 3.5 shows the solution of Algorithm 3.3.1 after 11 adaptive iterations. The Mach number is plotted in the figure. We observe the same stationary solution as in the related references. Dual solutions for drag and lift forces are plotted in the lower left and right plots, respectively.

Since we start with a coarse mesh, the mesh does not represent the surfaces of the airfoil accurately, see Figure 3.3 upper and lower-left plots. In order to decrease the geometry error, we project new points from the mesh refinement onto the original geometry, see Figure 3.3 lower-right plot. The finest meshes from the adaptive algorithm are presented in Figure 3.4. Refinements are strongly localized to the area with the largest error indicators.

Figure 3.5 shows the convergence results of the adaptive algorithm. We plot the values of the corresponding target functionals from each adaptive iteration together with the reference drag 0.022 and lift 0.344. We observe convergence of the algorithm already after six adaptive iterations. The values of the total error of the target functional is also presented. As the mesh gets finer, the total error approaches zero.

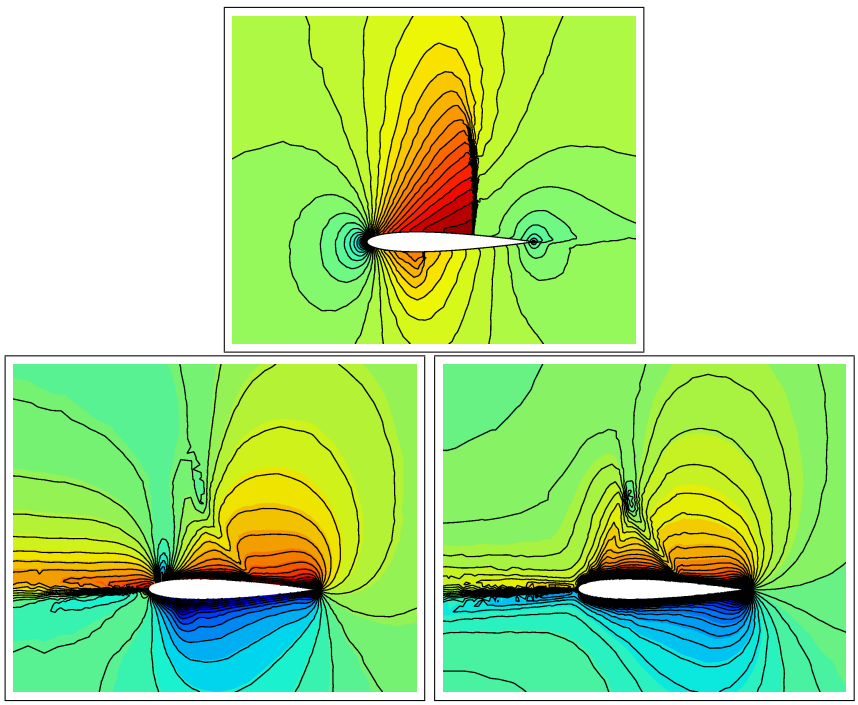

Figure 3.2. Naca 0012 airfoil: Mach number upper, x-component of dual momentum for the drag lower-left, and for the lift lower-right. Solutions obtained from the finest mesh with 10622 nodes, 20931 cells for the drag, and with 8567 nodes, 16837 cells for the lift.

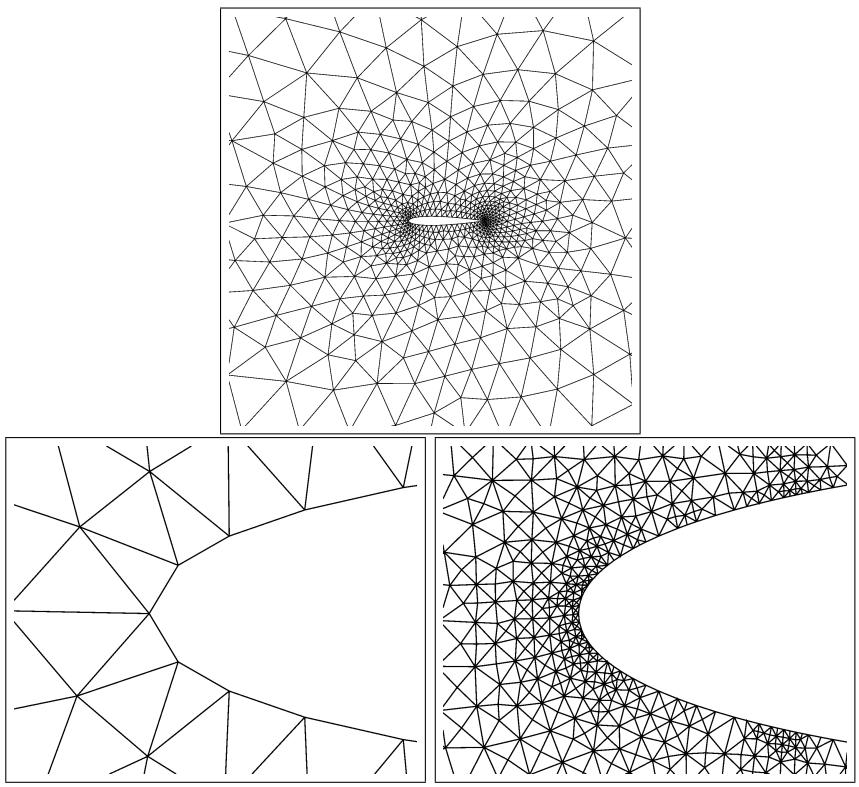

Figure 3.3. Naca 0012 airfoil: The initial mesh with 1114 nodes and 2136 cells, and the zoom of the finest mesh close to the leading edge.

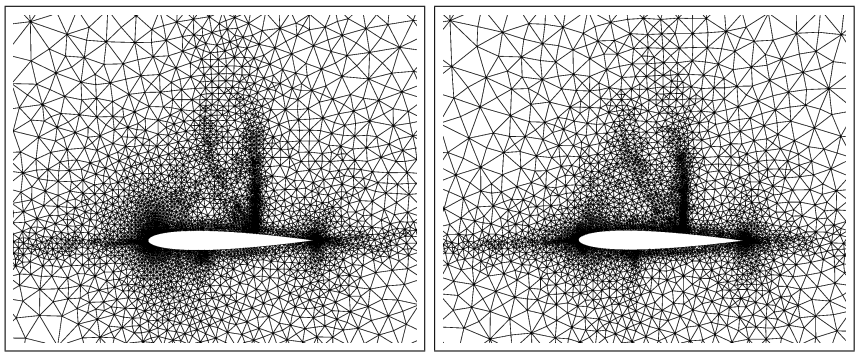

Figure 3.4. Naca 0012 airfoil: The finest mesh for the drag and lift functionals.

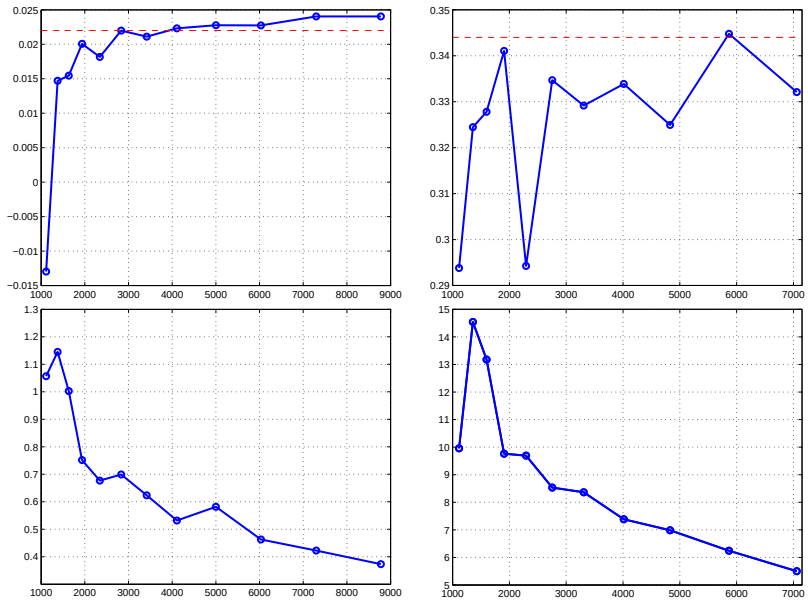

Figure 3.5. Naca 0012 airfoil: The values of the drag, top-left, and lift, top-right, coefficients from each adaptive iterations. The reference values, 0.022 and 0.344 respectively, are plotted in dashes. Corresponding error estimates as function of number of nodes are plotted below.

Chapter 4

Turbulence Simulation

The stabilized adaptive finite element method described in the chapters above offers an alternative approach to turbulence. With respect to a quantity of interest, the method adapts the mesh automatically based on a posteriori error estimation. Flow features are resolved which have large influence on the quantity of interest, while other small scale features remain unresolved with the stabilization acting as a subgrid model. Therefore, the adaptive method can be characterized as a DNS/LES method, since a part of the flow is resolved as a DNS (Direct Numerical Simulation) and the rest of the flow is left unresolved in a LES (Large Eddy Simulation). For example to compute mean value output for flow past a body, the method uses LES in the wake and DNS to capture separation and shocks. LES where the numerical method acts as subgrid model is called Implicit LES, see e.g. [73]. Adaptive mesh refinement based on rigorous error estimation significantly minimizes the computational cost of the simulation for turbulent flow. The dual problem shows sensitivity with respect to the output, which is taken into account automatically in the adaptive algorithm.

Adaptive DNS/LES was developed and successfully applied to incompressible flow by Hoffman and Johnson [74, 75, 76, 67, 77, 78, 79, 80, 81], which are also referred to as a *General Galerkin (G2) finite element method*. For a detailed analysis see [82].

4.1 Adaptive DNS/LES for compressible flows

In this thesis we study the extension of Adaptive DNS/LES to turbulent compressible flow. For low Mach numbers, the flow is characterized as in-

compressible since the effect of compressibility is negligible. However, when the Mach number increases the flow becomes very complex: including turbulent wakes, bow shocks, rarefaction waves, discontinuities, shock wake interaction, expansion and compression of supersonics regions, and transition to subsonic/supersonic flow. To resolve all these features by the numerical method is impossible for inviscid or slightly viscous flows. We can see in the above presented results in section 3.4 that the adaptive method focuses computational resources to regions that have high influence on the quantity of interest in the computation, thereby minimizing the computational cost.

The detailed discussion of the Adaptive DNS/LES method for compressible flow can be found in Papers III, IV, V and VI. Overall, Adaptive DNS/LES may open new possibilities for computational compressible turbulence.

4.2 Numerical Example

To illustrate some steps of the Adaptive DNS/LES, let us consider a subsonic $M = 0.1$ flow with Reynold's number $Re = 22000$ around a square cylinder, of diameter 0.0065 centered at $(0, 0, 0)$ inside a box of size $[-0.05, 0.15] \times [-0.026, 0.026] \times [0, 0.026]$, see Figure 4.1. The initial mesh has 26524 nodes and 139264 cells. We show results after 3 iterations of Algorithm 3.3.1, where the mesh has 48773 nodes and 255761 cells.

The slip boundary condition is used at the surfaces of the square cylinder and the walls. The characteristic boundary conditions are used at the inlet and outlet. After each time-step the values at the inflow boundary are corrected to have $\rho = 1.4$, $p = 1$, $\boldsymbol{u} = 0.1$. The upper plot of Figure 4.1 shows the contours of the magnitude of the vorticity and a colormap of the magnitude of the velocity. In the middle we plot the contours of the x-component of the dual momentum. The target functional of this problem is the drag force acting on the cylinder. After each step of Algorithm 3.3.1, the 10% of cells with the largest error contributions are marked for h-refinement. The lowest plot of Figure 4.1 shows the marked cells. As we can see, the refinement pattern of the algorithm does not follow the von Karman vortex street, instead it is localized to the area close to the cylinder. When we continue the steps until convergence for a given tolerance, some features of the flow will be resolved in a DNS, which have the highest contribution to the drag force. The rest is left unresolved in a LES.

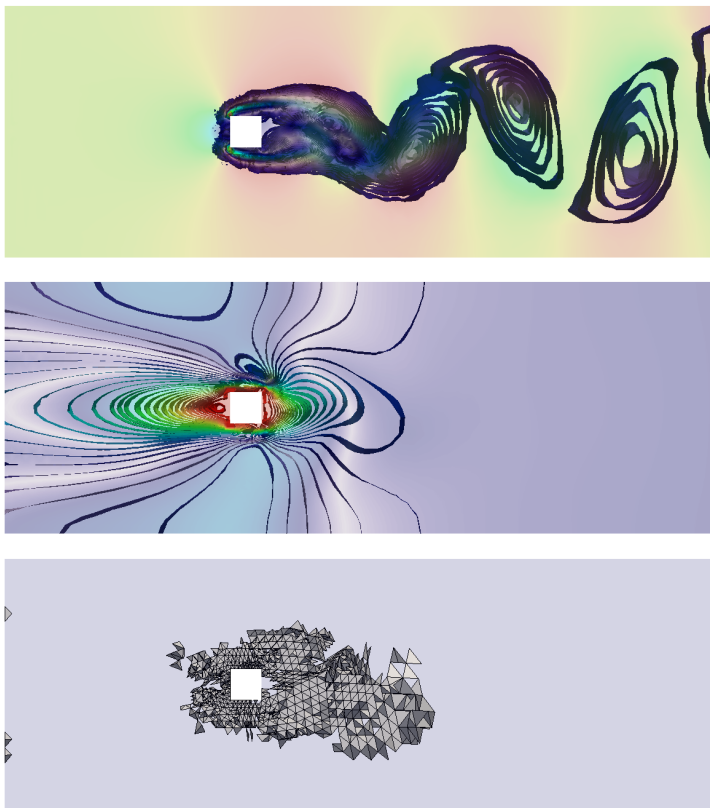

Figure 4.1. Adaptive DNS/LES for subsonic $M = 0.1$ flow around a square cylinder: vorticity contours together with the colormap of velocity magnitude at the top, contours and colormap of the x-component of the dual momentum in the middle, and 10% of the cells with the highest error contribution to the drag force at the bottom.

4.3 Summary of Paper VI

Paper VI combines the mathematical and computational results of the earlier papers to present an adaptive method for turbulent compressible flow. The stabilization of the equations is done by a residual based artificial viscosity presented in Paper II. We show that the artificial viscosity acts as a numerical stabilization, as shock-capturing and as turbulence capturing for large eddy simulation (LES) of turbulent flow. The adaptive method resolves parts of the flow indicated by the a posteriori error estimates, but leaves shocks and turbulence under-resolved in a LES. In the paper we review various approaches to LES for compressible turbulent flow, and we describe our approach and its similarities with existing methods. We simulate a 2D problem to show the performance of the stabilization and sharpness in shock capturing. Then we solve 3D problems: compressible flow around a circular cylinder and a sphere, for different Mach numbers. In the paper we use the drag coefficient as a target functional. We compare our results with experimental data, which is available in the literature.

Chapter 5

Conclusion and future direction

In this thesis we have developed three main contributions: a new high order stabilized method; a posteriori error estimates for time dependent compressible flows; and an adaptive DNS/LES approach for computing turbulent compressible flow.

Stabilized methods: the entropy viscosity method is extended in a more systematic way into the finite element framework; a residual based artificial viscosity method, is obtained by dropping least-square terms in the SD, GLS, SUPG methods, where the convergence for implicit schemes is proved for scalar conservation law in two space dimensions.

A posteriori error estimation: adjoint based a posteriori error estimates of target functionals are proved for time dependent compressible Euler/Navier-Stokes equations in 2D and 3D, using two approaches: primitive variables and conservation variables. Issues of stability of the computed dual solution in 2D for flow past a cylinder are investigated.

Adaptive DNS/LES is extended to simulate compressible turbulent flow. Realistic problems for different Mach numbers are solved and compared with experimental data.

The future work involves studying stability issues of the dual problem, parallelization and large scale turbulence computations.

Bibliography

[1] Hoffman J, Jansson J, Jansson N, Nazarov M. *Unicorn project*. `https://launchpad.net/unicorn`, 2011.

[2] FEniCS. *FEniCS project*. `http://www.fenicsproject.org`, 2003.

[3] Leray J. Sur le mouvement d'un liquide visquex emplissent l'espace. *Act aMat h.* 1934; **63**:193–248.

[4] Ladyzhenskaya O. *The Mathematical Theory of Viscous Incompressible Flows (2nd edition)*. Gordon and Breach, 1969.

[5] LeVeque RJ. *Finite Volume Methods for Hyperbolic Problems*. Cambridge University Press, 2002.

[6] Woodward P, Colella P. The numerical simulation of two-dimensional fluid flow with stong shocks. *Journal of Computational Physics* 1984; **54**:115–173.

[7] Godunov SK. A difference scheme for numerical solution of discontinuous solution of hydrodynamic equations. Math. Sbornik (1959), translated US Joint Publ. Res. Service, JPRS 7226, 1969; 271–306.

[8] van Leer B. Towards the ultimate conservative difference scheme. v. a second order sequel to godunov's methods. *J. Comput. Phys.* 1979; **32**:101–136.

[9] Neumann JV, Richtmyer R. A method for the numerical calculation of hydrodynamic shocks. *J. Appl. Phys.* 1950; **21**:232–237.

[10] Harten A. Adaptive multiresolution schemes for shock computations. *J. Comput. Phys* 1994; **115**:319–338.

[11] Arnold DN, Brezzi F, Cockburn B, Marini LD. Unified analysis of discontinuous galerkin methods for elliptic problems. *Siam Journal on Numerical Analysis* 2002; **39**, doi:10.1137/S0036142901384162.

[12] Patera AT. A spectral element method for fluid dynamics: Laminar flow in a channel expansion. *Journal of Computational Physics* 1984; **54**:468–488, doi:10.1016/0021-9991(84)90128-1.

[13] Brooks A, TJR Hughes. Streamline upwind/petrov- galerkin formulations for convection dominated flows with particular emphasis on the incompressible navier-stokes equations 1982; **32**:199–259.

[14] Hughes T, Brooks A. A multi-dimensional upwind scheme with no crosswind diffusion, in: Finite element methods for convection dominated flows. T.J.R. Hughes (ed.), ASME Monograph AMD-34, 1979; 19–35.

[15] Hughes T, Tezduyar T. Finite element methods for first-order hyperbolic systems with particular emphasis on the compressible euler equations. *Computer methods in applied mechanics and engineering* 1984; **45**:217–284.

[16] Tezduyar T, Senga M. Stabilization and shock-capturing parameters in SUPG formulation of compressible flows. *Computer Methods in Applied Mechanics and Engineering* 2006; **195**:1621–1632.

[17] Hughes TJR, Scovazzi G, Tezduyar TE. Stabilized methods for compressible flows. *Journal of Scientific Computing* 2008; .

[18] Johnson C, U Nävert. An analysis of some finite element methods for advection diffusion problems. Analytical and Numerical Approaches to Asymptotic Problems in Analysis. Axelsson, S. et all (eds.), North-Holland, 1981.

[19] U Nävert. A finite element method for convection-diffusion problems. PhD Thesis, Chalmers TU, Goteborg, 1982.

[20] Johnson C, U Nävert, J Pitkäranta. Finite element methods for linear hyperbolic problems 1984; **45**:285–312.

[21] Johnson C, JSaranen. Streamline diffusion methods for the incompressible euler and navier-stokes equations 1986; **47**:1–18.

[22] Johnson C, Szepessy A. *Shock-capturing streamline diffusion finite element methods for nonlinear conservation laws.* Recent Developments in Computatioonal Fluid Dynamics, edited by T. J. R. Hughes and T. Tezduyar, AMD-Vol 95, 1988.

[23] Johnson C, Szepessy A, Hansbo P. On the convergence of shock-capturing streamline diffusion finite element methods for hyperbolic conservation laws. *Mathematics of Computation* 1990; **54(189)**:107–129.

[24] Hansbo P. Explicit streamline diffusion finite element methods for the compressible euler equations in conservation variables. *Journal of Computational Physics* 1993; **109**:274–288.

[25] Guermond JL. Stabilization of Galerkin approximations of transport equations by subgrid modeling. *M2AN* 1999; **33(6)**:1293–1316.

[26] Guermond JL. Subgrid stabilization of galerkin approximations of monotone operators. *IMA J. Numer. Anal.* 2001; **21**:165–197.

[27] Hughes TJR, Feijóo GR, Mazzei L, Quincy JB. The variational multiscale method - a paradigm for computational mechanics. *Computer methods in applied mechanics and engineering* 1998; **166**:3–24.

[28] Hughes TJR, Mazzei L, Jansen KE. Large eddy simulation and the variational multiscale method. *Computer methods in applied mechanics and engineering* 2000; **3**:47–59.

[29] Hughes TJR, Mazzei L, Jansen KE. Large eddy simulation of turbulent channel flows by the variational multiscale method. *Physics of Fluids* 2001; **13**:1784–1799.

[30] Bazilevs Y, Calo V, Cottrell J, Hughes T, Reali A, Scovazzi G. Variational multiscale residual-based turbulence modeling for large eddy simulation of incompressible flows. *Computer methods in applied mechanics and engineering* 2007; **197(1-4)**:173–201.

[31] Burman E, Hansbo P. Edge stabilization for Galerkin approximations of convection-diffusion-reaction problems. *Comput. Methods Appl. Mech. Eng.* 2004; **193**(15-16):1437–1453.

[32] Burman E, Hansbo P. Edge stabilization for the generalized stokes problem: A continuous interior penalty method. *Computer Methods in Applied Mechanics and Engineering* 2006; **195**(19-22):2393 – 2410, doi:DOI: 10.1016/j.cma.2005.05.009.

[33] Guermond JL, Pasquetti R. Entropy-based nonlinear viscosity for fourier approximations of conservation laws. *C. R. Acad. Sci.* 2008; **Ser. I, 346**:801–806.

[34] Guermond JL, Pasquetti R, Popov B. Entropy viscosity method for nonlinear conservation laws. *J. Comput. Phys.* 2011; **230(2011)**:4248–4267.

[35] Guermond JL, Nazarov M, Popov B. Implementation of the entropy viscosity method. *submitted* 2011; .

[36] Löhner R. An adaptive finite element scheme for transient problems in cfd. *Computer Methods in Applied Mechanics and Engineering* 1987; **61**(3):323–338, doi:DOI: 10.1016/0045-7825(87)90098-3.

[37] Hirsch C. *Computational methods for inviscid and viscous flows: Numerical Computation of Internal and External Flows, vol. 2,*. John Wiley & Sons, 1990.

[38] Szepessy A. Convergence of a shock-capturing streamline diffusion finite element method for a scalar conservation law in two space dimensions. *Mathematics of Computation* 1989; **53**:527–545.

[39] Szepessy A. Convergence of a streamline diffusion finite element method for scalar conservation laws with boundary conditions. *Mathematical Modelling and Numerical Analysis* 1991; **25**:749–782.

[40] Johnson C, Szepessy A, Hansbo P. On the convergence of shock-capturing streamline diffusion finite element methods for hyperbolic conservation laws. *Mathematics of Computation* 1990; **54(189)**:107–129.

[41] John V. Slip with friction and penetration with resistance boundary conditions for the navier–stokes equations - numerical tests and aspects of the implementation. *J. Comp. Appl. Math* 2002; **147**:287–300.

[42] Lohner R. *Applied CFD techniques: an introduction based on finite element methods*. John Wiley & Sons, 2001.

[43] Eriksson K, Johnson C. An adaptive finite element method for linear elliptic problems. *Math. Comp.* 1988; **50**:361–383.

[44] Estep D. A short course on duality, adjoint operators, green's functions, and a posteriori error analysis. Department of Mathematics, Colorado State University, Agust 6, 2004.

[45] Babuška I. *Feedback, adaptivity and a posteriori estimates in finite elements: Aims, theory, and experience*. Accuracy, Estimates and Adaptive Refinements in Finite Element Computation (I. Babuška, O. C. Zienkiewicz, J. Gago, and E. R. de A. Oliveira eds.), Wiley, New York, 1986.

[46] Babuška I, Miller A. The post-processing approach in the finite element method—part 3:a posteriori error estimates and adaptive mesh selection. *International Journal for Numerical Methods in Engineering* 1984; **20**:2311–2324, doi:10.1002/nme.1620201211.

[47] Eriksson K, Estep D, Hansbo P, Johnson C. Introduction to adaptive methods for differential equations. *Acta Numer.* 1995; **4**:105–158.

[48] Eriksson K, Estep D, Hansbo P, Johnson C. *Computational Differential Equations*. Cambridge University Press New York, 1996.

[49] Becker R, Rannacher R. A feed-back approach to error control in adaptive finite element methods: Basic analysis and examples. *East-West J. Numer. Math.* 1996; **4**:237–264.

[50] Becker R, Rannacher R. A posteriori error estimation in finite element methods. *Acta Numer.* 2001; **10**:1–103.

[51] Johnson C, Rannacher R. Numerics and hydrodynamic stability: Towards error control in cfd. *SIAM J. Numer. Anal.* 1995; **32**:1058–1079.

[52] Giles M, Süli E. Adjoint methods for pdes: a posteriori error analysis and postprocessing by duality. *Acta Numer.* 2002; **11**:145–236.

[53] Oden JT, Prudhomme S. On goal-oriented error estimation for elliptic problems: Application to the control of pointwise errors. *Comput. Meth. Appl. Mech. Eng.* 1999; **111**:185–202.

[54] Oden JT, Prudhomme S. *Computable error estimators and adaptive techniques for fluid flow problems*. Error Estimation and Solution Adaptive Discretization in Computational Fluid Dynamics (Ed. T. J. Barth and H. Deconinck), Lecture Notes in Computational Science and Engineering, Springer-Verlag Publishing: Heidelberg, 2002.

[55] Ainsworth M, Oden JT. A posteriori error estimation in finite element analysis. *Computat. Meth. Appl. Mech. Eng.* 1997; **142**:1–88.

[56] Paraschivoiu M, Peraire J, Patera AT. A posteriori finite element bounds for linear-functional outputs of elliptic partial differential equations. *Comput. Meth. Appl. Mech. Eng.* 1997; **150**:289–312.

[57] Babuška I, Guo BQ. The h, p and h-p version of the finite element method; basis theory and applications. *Advances in Engineering Software* 1992; **15**(3-4):159 – 174, doi:DOI: 10.1016/0965-9978(92)90097-Y.

[58] Babuška I, Suri M. The p and h-p versions of the finite element method, basic principles and properties. *SIAM Rev.* December 1994; **36**:578–632, doi:10.1137/1036141.

[59] Johnson C, Szepessy A. Adaptive finite element methods for conservation laws based on a posteriori error estimates. *Communications on Pure and Applied Mathematics* ; **48**:199–234, doi:10.1002/cpa.3160480302.

[60] Johnson C. *Adaptive Finite Element Methods for Conservation Laws*. Advanced Numerical Approximation of Nonlinear Hyperbolic Equations, Springer Lecture Notes in Mathematics, Springer Verlag, 1998; 269–323.

[61] Hartmann R. Adaptive FE Methods for Conservation Equations. *Hyperbolic Problems: theory, numerics, applications: eighth international conference in Magdeburg, February, March 2000*, *International series of numerical mathematics*, vol. 141, Freistühler H, Warnecke G (eds.), Birkhäuser, Basel, 2001; 495–503.

[62] Houston P, Hartmann R. Goal–oriented a posteriori error estimation for compressible fluid flows. *Numerical Mathematics and Advanced Applications*, Brezzi F, Buffa A, Corsaro S, Murli A (eds.), Springer, 2003; 775–784.

[63] Houston P, Hartmann R, Süli A. Adaptive discontinuous Galerkin finite element methods for compressible fluid flows. *Numerical methods for Fluid Dynamics VII, ICFD*, Baines M (ed.), 2001; 347–353.

[64] Larson M, Barth T. A posteriori error estimation for discontinuous galerkin approximations of hyperbolic systems. *In Discontinuous Galerkin Methods, B. Cockburn, G. Karniadakis, and C.-W. Shu, editors, Lecture Notes in Comput. Sci. Engrg., 11, Springer, Berlin*, 2000; 363–368.

[65] Burman E. Adaptive finite element methods for compressible flow. *Computer methods in applied mechanics and engineering* 2000; **190**:1137–1162.

[66] Nazarov M, Hoffman J. An adaptive finite element method for inviscid compressible flow. *International Journal for Numerical Methods in Fluids* 2010; **64**(10-12):1102–1128, doi:10.1002/fld.2335. URL `http://dx.doi.org/10.1002/fld.2335`.

[67] Hoffman J. Computation of mean drag for bluff body problems using adaptive dns/les. *SIAM J. Sci. Comput.* 2005; **27(1)**:184–207.

[68] Hoffman J, Johnson C. A new approach to computational turbulence modeling. *Compit. Meth. Appl. Engrg* 2006; **195**:2865–2880.

[69] Hoffman J. Adaptive simulation of the turbulent flow past a sphere. *J. Fluid Mech.* 2006; **568**:77–88.

[70] Hoffman J. Efficient computation of mean drag for the subcritical flow past a circular cylinder using general galerkin G2. *International Journal of Numerical Methods in Fluids* 2009; **59(11)**:1241–1258.

[71] Hartmann R, Houston P. Adaptive discontinuous galerkin finite element methods for the compressible euler equations. *J. Comput. Phys.* 2002; **183**:508–532.

[72] Venditti DA, Darmofal DL. Grid adaptation for functional outputs: application to two-dimensional inviscid flows. *J. Comput. Phys* 2002; **176**:40–69.

[73] Sagaut P. *Large Eddy Simulation for Incompressible Flows*. Springer-Verlag, Berlin, Heidelberg, New York, 2001.

[74] Hoffman J. On duality based a posteriori error estimation in various norms and linear functionals for les. *SIAM J. Sci. Comput.* 2004; **26(1)**:178–195.

[75] Hoffman J. Efficient computation of mean drag for the subcritical flow past a circular cylinder using general galerkin G2. *International Journal of Numerical Methods in Fluids* 2009; **59(11)**:1241–1258.

[76] Hoffman J, Johnson C. Stability of the dual navier-stokes equations and efficient computation of mean output in turbulent flow using adaptive dns/les. *Comput. Methods Appl. Mech. Engrg.* 2006; **195**:1709–1721.

[77] Hoffman J, Johnson C. *Adaptive DNS/LES: a New Agenda in CFD*. Finite Element Methods: 1970s and beyond, CIMNE, 2004.

[78] Hoffman J. Adaptive turbulence computation based on weak solutions and weak uniqueness, quality and reliability of large-eddy simulations. *Eds. J. Meyers, B.J. Geurts and P. Sagaut* 2008; :21–35.

[79] Hoffman J. Adaptive simulation of the sub-critical flow past a sphere. *J. Fluid Mech.* 2006; **568**:77–88.

[80] Hoffman J. Computation of turbulent flow past bluff bodies using adaptive general galerkin methods: drag crisis and turbulent euler solutions. *Comp. Mech.* 2006; **38**:390–402.

[81] Hoffman J, Johnson C. A new approach to computational turbulence modeling. *Compit. Meth. Appl. Engrg* 2006; **195**:2865–2880.

[82] Hoffman J, Johnson C. *Computational Turbulent Incompressible Flow.* Springer, 2007.

Part II

Included Papers